Experimental Validation of a Structural Glass Window Design for In-plane Seismic Strengthening

Numerical predictions and experimental validation of unreinforced masonry structures in Groningen area

Appendix: Final Version
Master Thesis
Mehmet Kisa
03-08-2021

Table of Contents

A. Numerical analysis

A.1 Stress analysis

A.1.1. Model 1

Relative Interface Displacement	Maximum Stress Glass
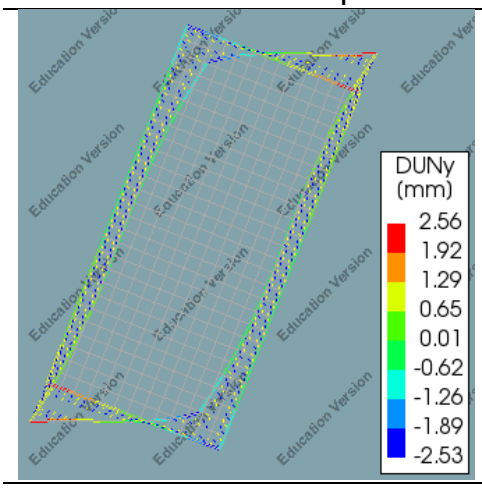	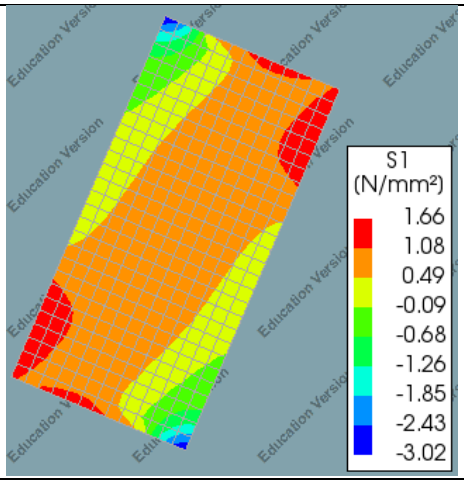
Total Displacement: 13.2 mm Relative Interface displacement: +2,5 mm	
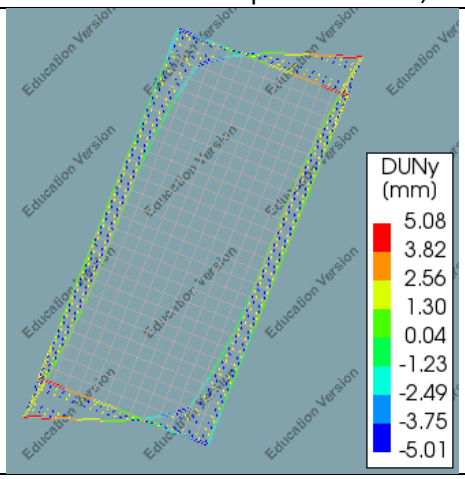	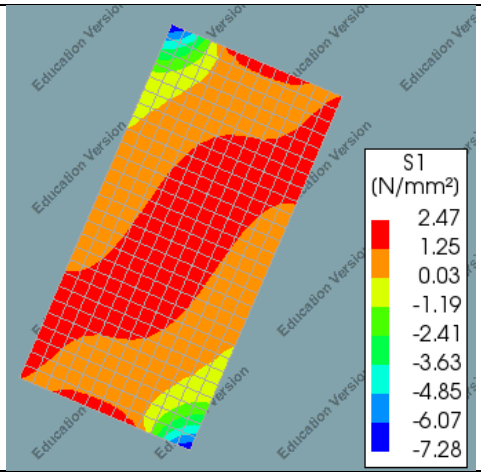
Total Displacement: 25.8 mm Relative Interface Displacement: -5 mm	
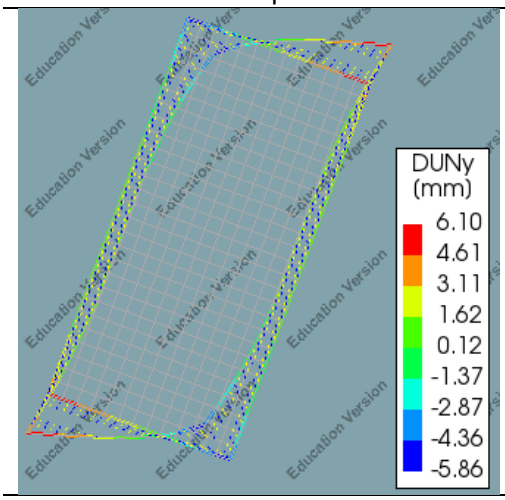	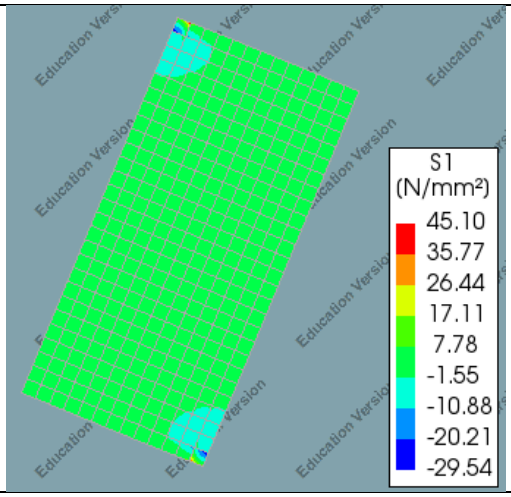
Total Displacement: 33 mm	Maximum stress: +45 MPa

Table 1: Relative interface displacement vs stresses in the glass for model 1

A.1.2. Model 2

Relative Interface Displacement	Maximum Stress Glass
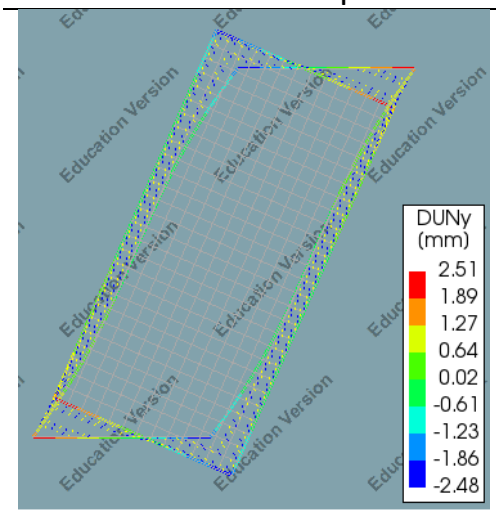	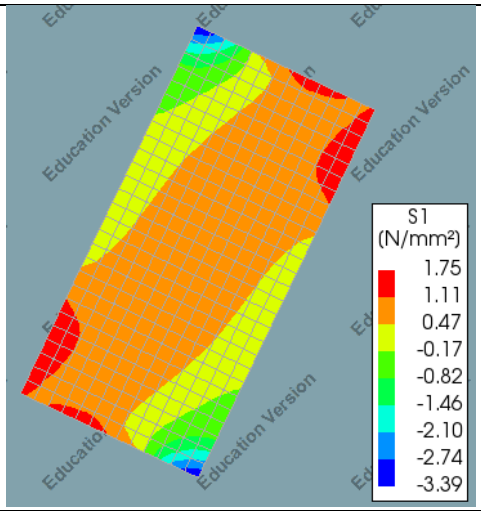
Total Displacement: 13.2 mm Relative Interface displacement: +2,5 mm	
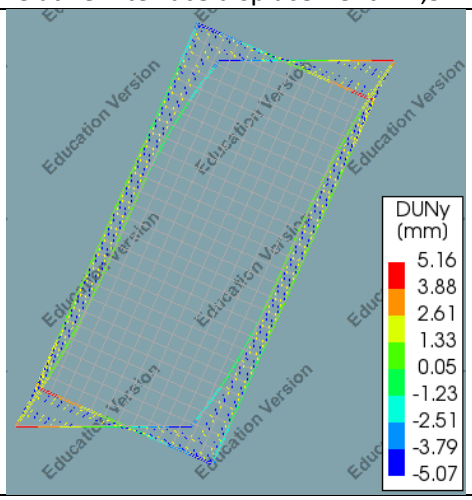	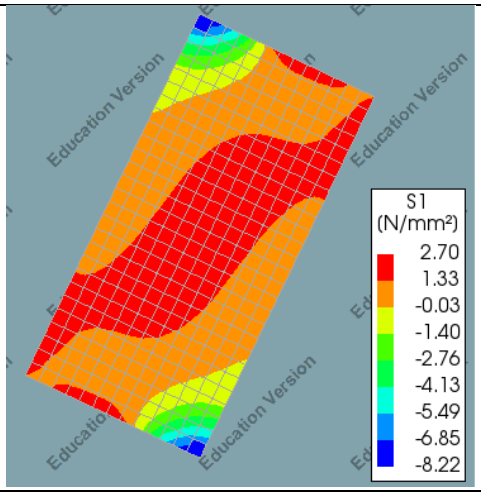
Total Displacement: 27 mm Relative Interface Displacement: -5 mm	
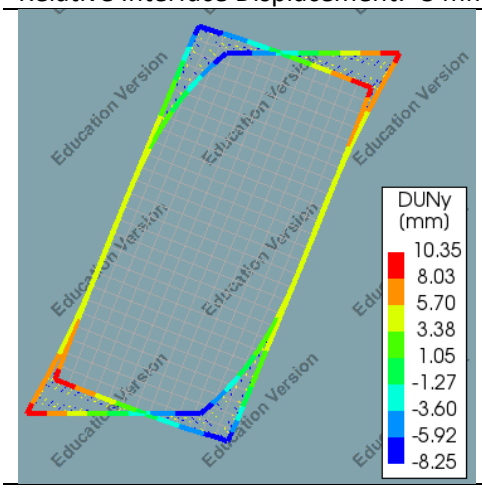	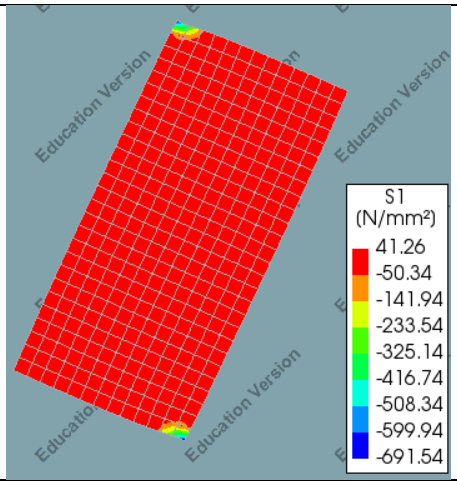
Total Displacement: 60 mm	Maximum stress: +41MPa

Table 2: Relative interface displacement vs stresses in the glass for model 2

A.1.3. Model 3

Relative Interface Displacement	Maximum Stress Glass
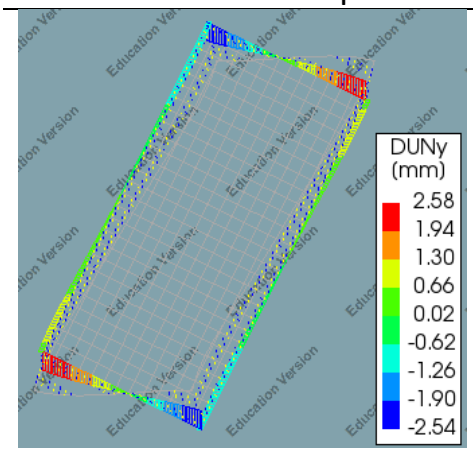	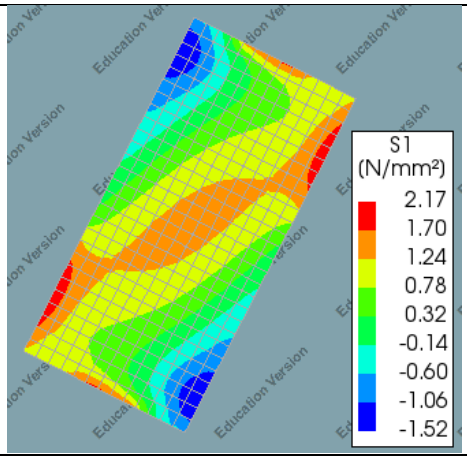
Total Displacement: 12 mm Relative Interface displacement: +2,5 mm	
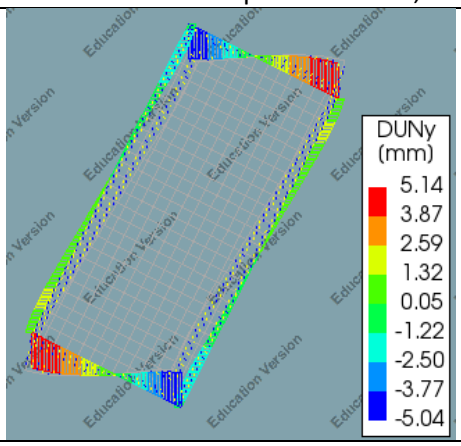	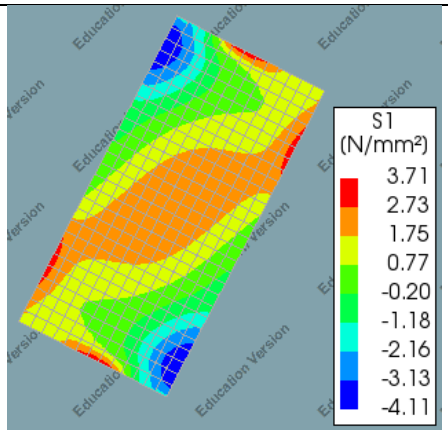
Total Displacement: 23.4 mm Relative Interface Displacement: -5 mm	
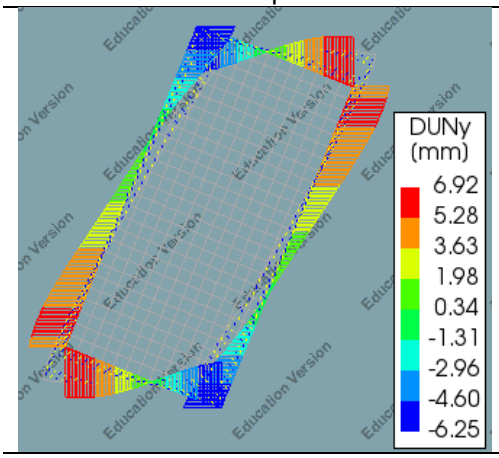	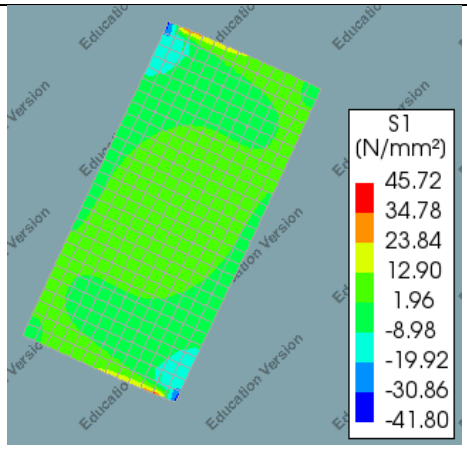
Total Displacement: 39 mm	Maximum stress: +45 MPa

Table 3:: Relative interface displacement vs stresses in the glass for model 3

A.2 Material model analysis

Test model Coulomb Friction

To start with, the interface is modelled for a basic model with two blocks. The interface is placed in between the two blocks as is seen in Figure 1. This test model will be loaded for a tension, shear and compression load for the Coulomb friction model using a gap model with shear retention, to see its structural influence. A non-linear soil bedding model will also be analysed for a compression load. Since this model is mostly interesting for compression loads. See Table 4 for an overview of the different test models.

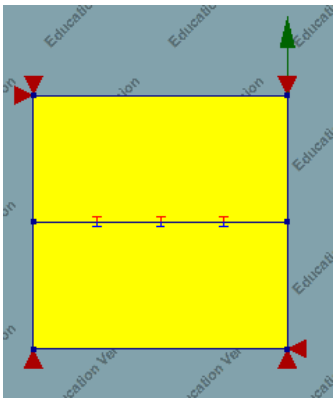

Figure 1 :Numerical model of the test model

Coulomb model 1: Gap model – Shear force	Coulomb model 2: Gap model – Tension force	Coulomb model 3: Gap model – compression force	Coulomb model 4: Soil bedding – Compression force
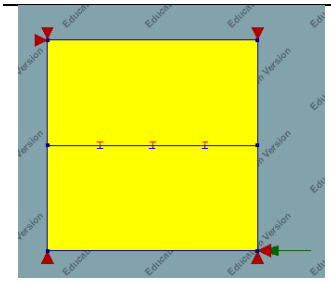	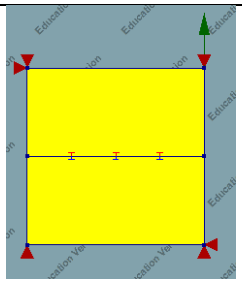	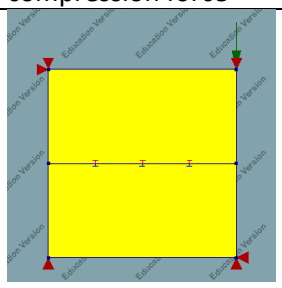	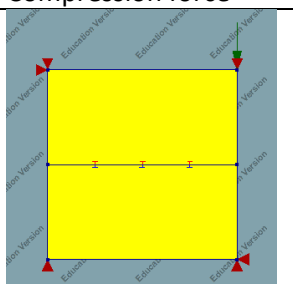

Table 4:Overview of the different test models

In Table 5 the material properties of the adhesive are shown for the test models. Coulomb model 1, Coulomb model 2 and Coulomb model 3 have the same material properties. Since only the load is changing. Model 4 uses nonlinear soil bedding as the interface opening and therefore has different material properties. The cohesion factor, friction angle and dilatancy angle are significantly low in this model. By doing so, the plastic behaviour will be visible in the results. The maximum compressive stress and unloading-reloading normal stiffness are determined by trial and error.

	Coulomb Model 1,2,3	Coulomb Model 4
Cohesion (N/mm^2)	1	1
Friction angle (°)	0.1	0.1
Dilatancy angle (°)	0	0
Interface opening	Gapping model	Nonlinear soil bedding
Tensile strength (N/mm^2)	1	-
Model for gap appearance	Constant shear retention	-
Reduced shear stiffness (N/mm^3)	1	-
Unloading-reloading normal stiffness (N/mm^3)	-	100
Maximum compressive stress (N/mm^2)	-	20

Table 5: Material properties for the adhesive

In Table 6 the analysis methods of the test models are shown. The analysis methods of all models are very similar however, the load varies. The displacement load for mode 1 is 40 mm, while for model 2 it is 10 mm. The plastic behaviour for model 1 was not visible for the same displacement as for model 2. This is why the displacement load is taken differently. The same reasoning is used for the other models.

		C. Model 1	C. Model 2	C. Model 3	C. Model 4
Load	Load name	Cyclic shear load	Cyclic tension load	Cyclic compression load	Cyclic compression load
	Load	40 mm	10 mm	20 mm	10 mm
	Load step	0.01(100) -0.01(100)	0.01(100) -0.01(100)	0.01(100) -0.01(100)	0.01(100) -0.01(100)
Iterative procedure	Procedure	Regular Newton-Raphson	Regular Newton-Raphson	Regular Newton-Raphson	Regular Newton-Raphson
	Max. number of iterations	50	50	50	50
	Line search	No	No	No	No
Convergence criterium	Norm	Force & Displacement	Force & Displacement	Force & Displacement	Force & Displacement
	Tolerance	0.01	0.01	0.01	0.01
	No convergence	Terminate	Terminate	Terminate	Terminate

Table 6: Analysis of the test models

Results

In Figure 2 the displacement curves of the test models are shown. From the displacement curve of model 1, the plastic behaviour due to the horizontal loading is visible. This means that the shear stiffness reduces when the maximum shear stress is reached.

From the displacement curve of model 2, the tearing of the adhesive due to tearing is visible. The tearing decreases the stiffness of the model. When the model is reloaded, the model will have the same stiffness as the reduced stiffness of the model. Thus, since the tearing already occurred in the first loading, the tearing will not continue and the stiffness will not decrease further for the same displacement.

From the displacement curve of model 3 strength reduction for the unloading and reloading is not visible. The unloading curve is the same line back. Furthermore, there is no increase in stiffness due to contact between the two blocks. This would be a problem in the window frame model since the contact between the glass panel and the timber frame is crucial.

From the displacement curve of model 4, the strength reduction for the unloading is visible. However, reloading it does not give the same results.

Using both material models for the structural window frame will conclude whether the Coulomb friction model is a suitable material model to use for cyclic loading for the structural window frame. This is investigated in the main report.

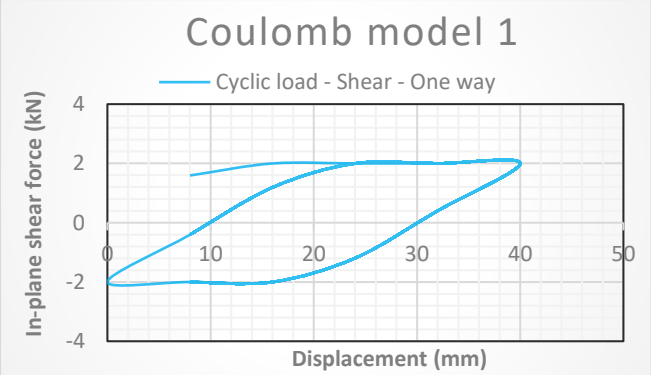

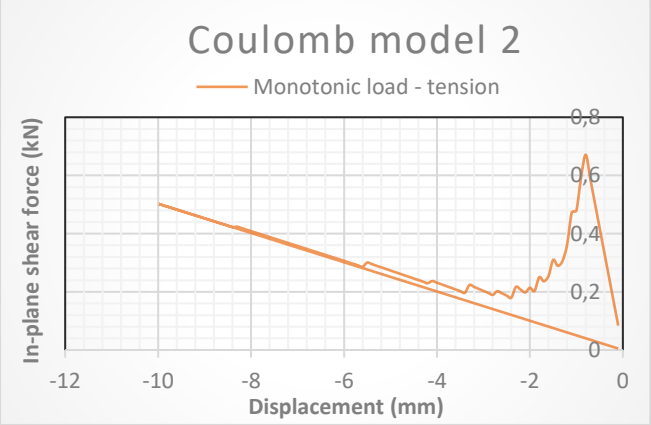

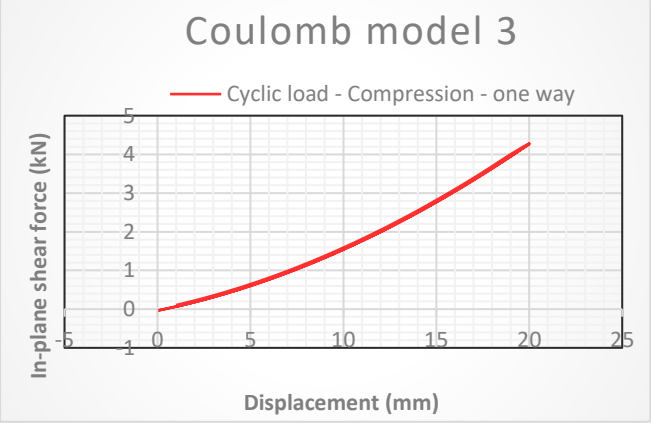

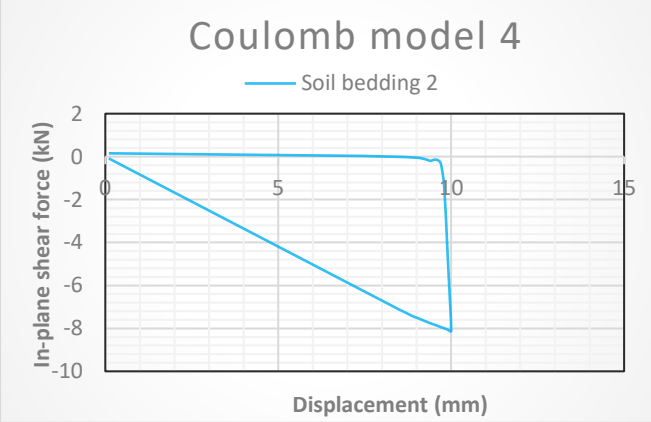

Figure 2: Displacement curves of the test models

Test model Mooney-Rivlin

Similarly, to the Coulomb Friction model, the Mooney-Rivlin model is also modelled with only two timber blocks. The model is made using plane strain elements since this is required for the Mooney-Rivlin model. It is noticeable that the adhesive is modelled by using a polygon sheet, see Figure 3.

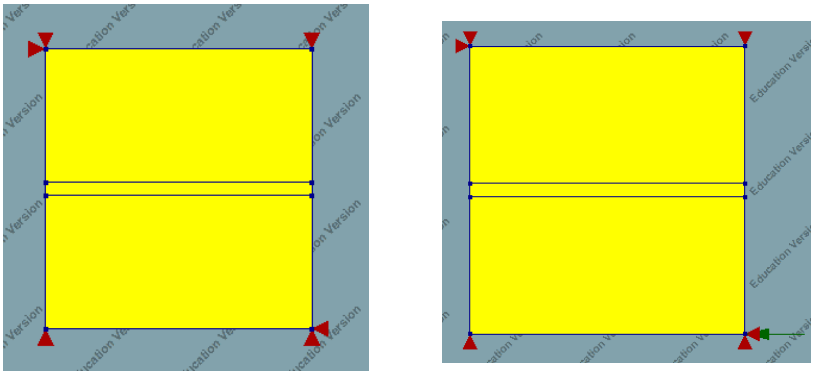

Figure 3: Numerical test model Mooney-Rivlin

The material properties of the blocks are less important. For this model, a timber block is assumed. A horizontal displacement load of 40 mm, which goes forth and back, is placed to measure the effect on the adhesive. For the material properties of the adhesive, a Deviatoric model of Mooney-Rivlin is used. Mooney-Rivlin is an option within composite rubber materials, where the option hyperelasticity and rubber is used. The value of K1 = 0.33 MPa and K2 = 0.05 MPa with Linear compressibility and a Bulk Modulus of 10 MPa.

Results

The results show a linear behaviour for the shearing of the adhesive. There is no tearing of the adhesive or plastic behaviour visible. Using this adhesive for the structural window frame would conclude whether this material model is usable.

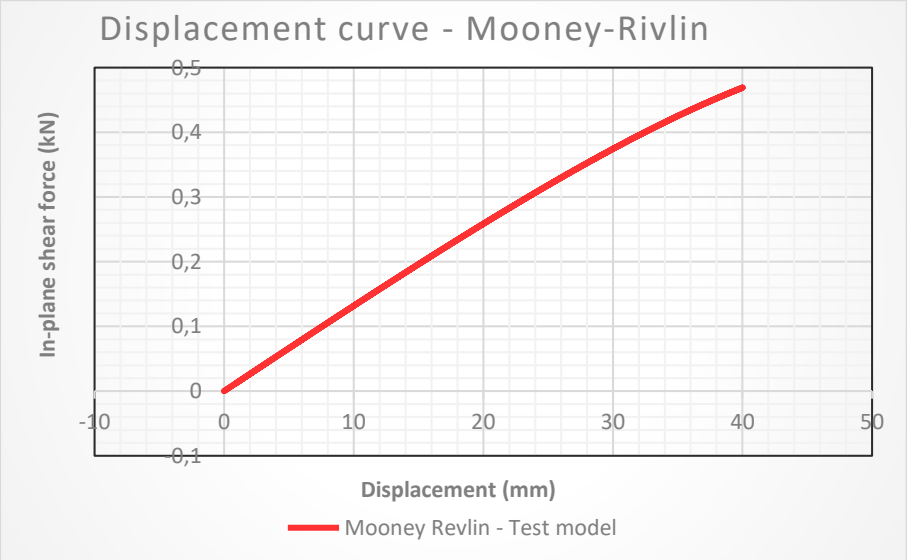

Figure 4:Displacement curve Mooney Rivlin - Test model

A.3 Mesh Analysis

Model 1

A.2.1 Mesh 50 mm

Relative interface displacement	Stress glass panel	Stress timber frame
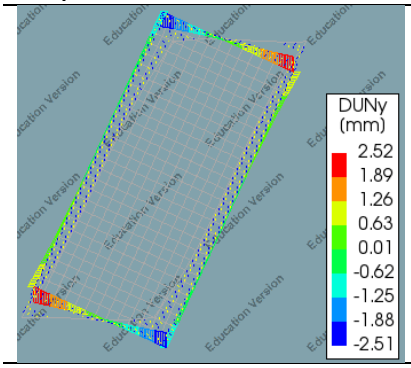	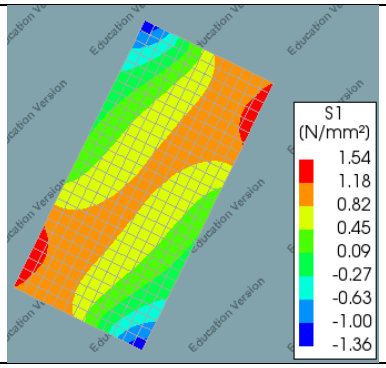	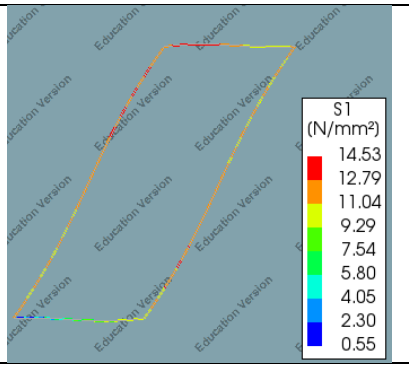
Total displacement 12.6 mm Relative interface displacement: +2,5 mm		
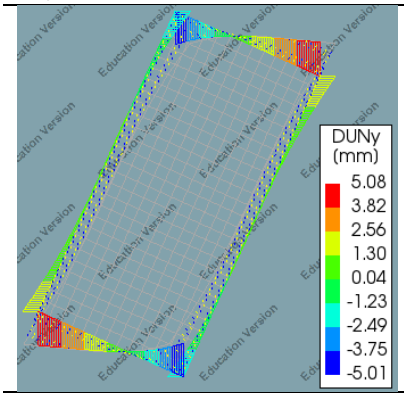	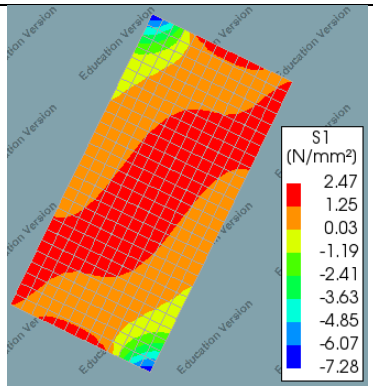	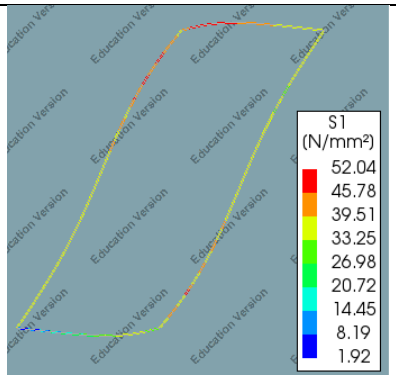
Total displacement: 25.8 mm Relative interface displacement: -5 mm		
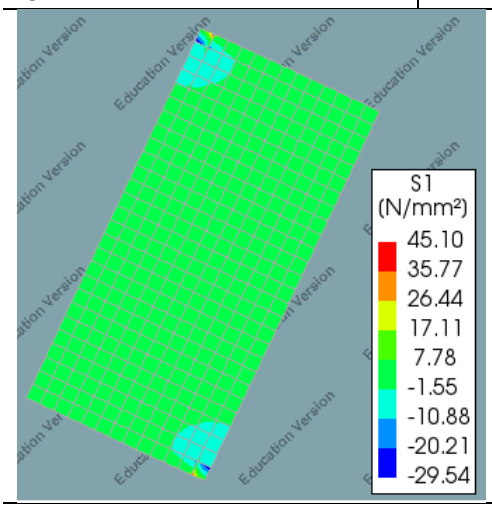	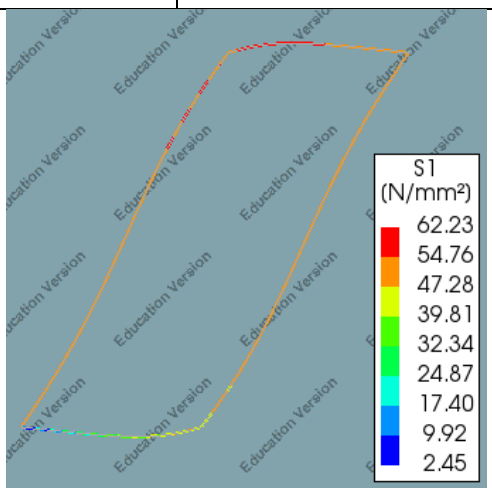	
Total displacement 33 mm Maximum stress: +45 MPa		

Table 7: Computational results of a mesh of 50 mm

A.2.2 Mesh 25 mm

Relative interface displacement	Stress glass panel	Stress timber frame
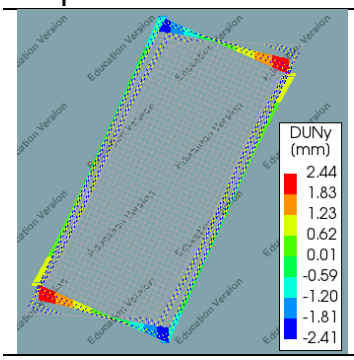	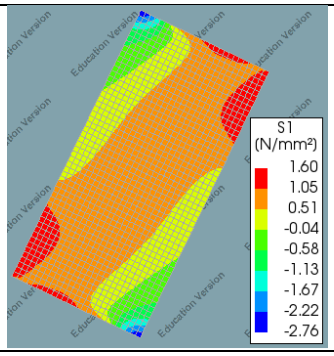	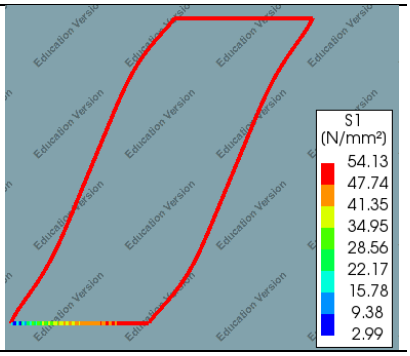
Total displacement 12.6 mm Relative interface displacement: +2,5 mm		
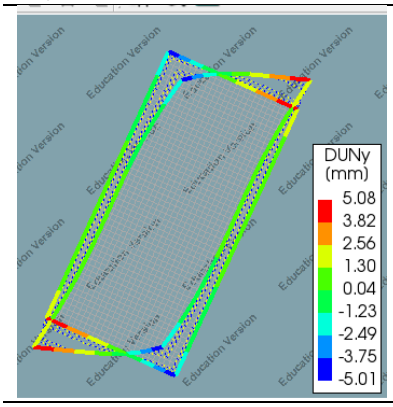	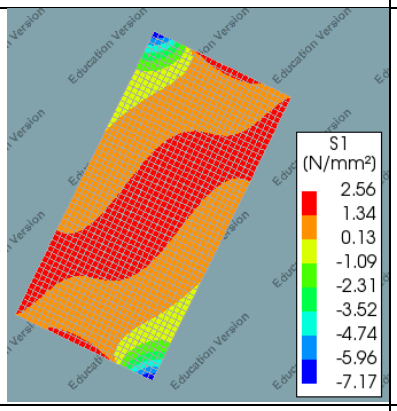	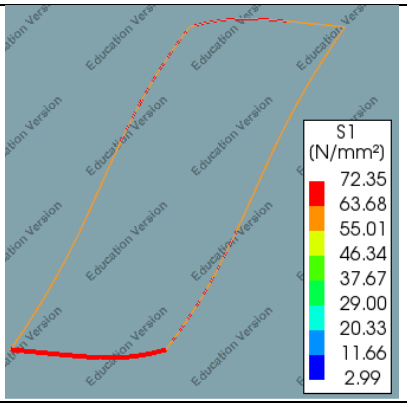
Total displacement: 25.8 mm Relative interface displacement: -5 mm		
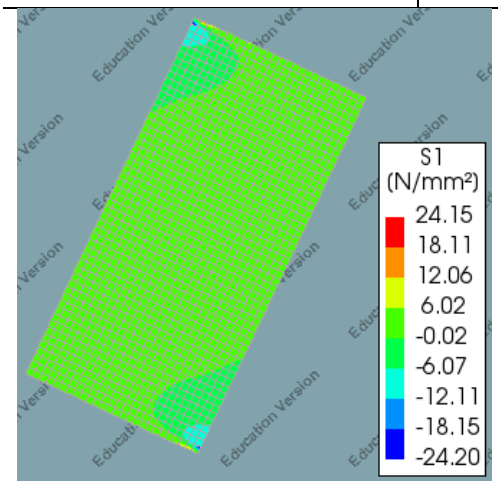	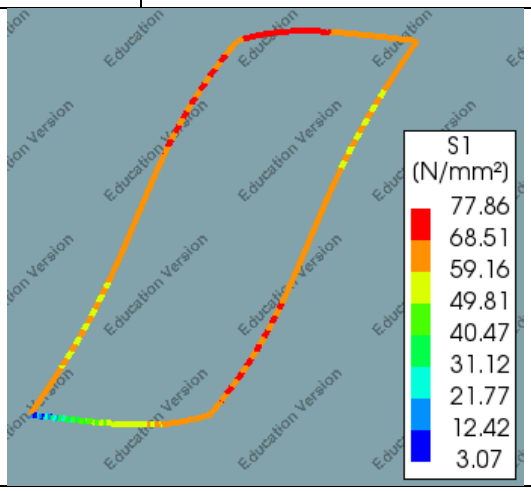	
Total displacement 33 mm		

Table 8: Computational results of a mesh of 25 mm

A.2.3 Mesh 100 mm

Relative interface displacement	Stress glass panel	Stress timber frame
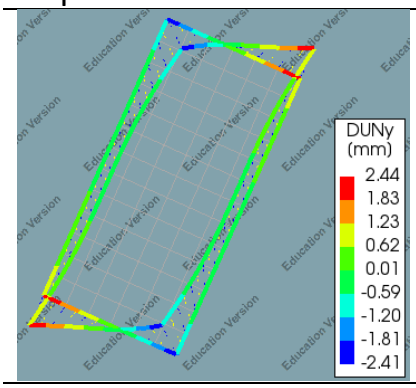	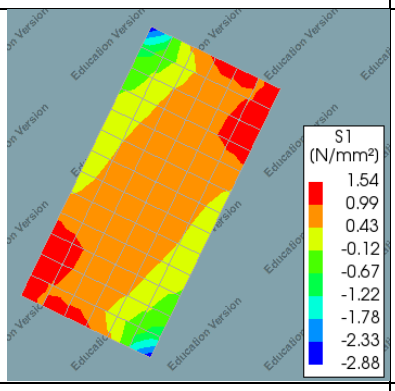	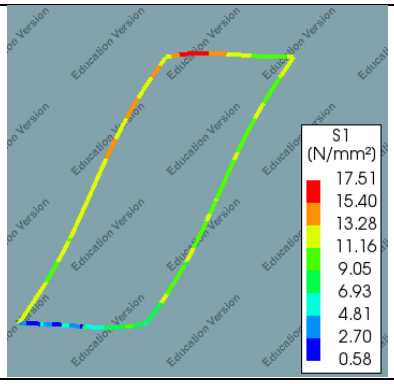
Total displacement 12.6 mm Relative interface displacement: +2,5 mm		
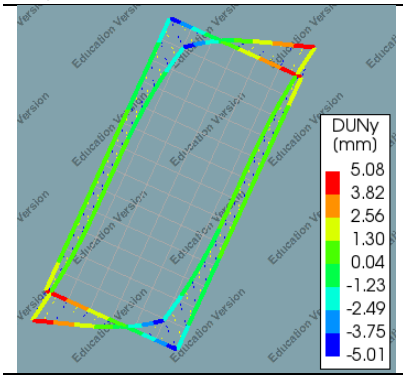	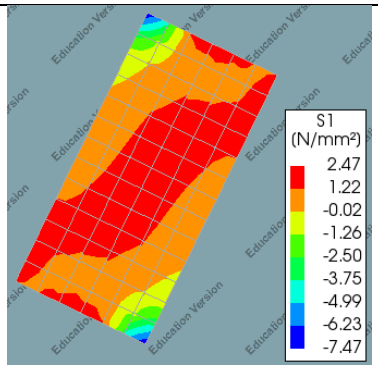	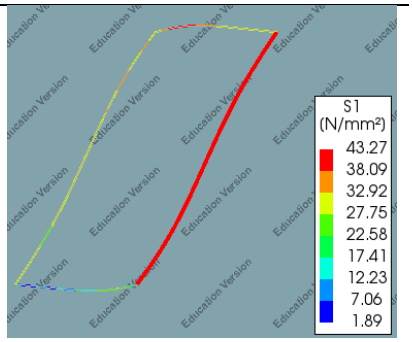
Total displacement: 25.8 mm Relative interface displacement: -5 mm		
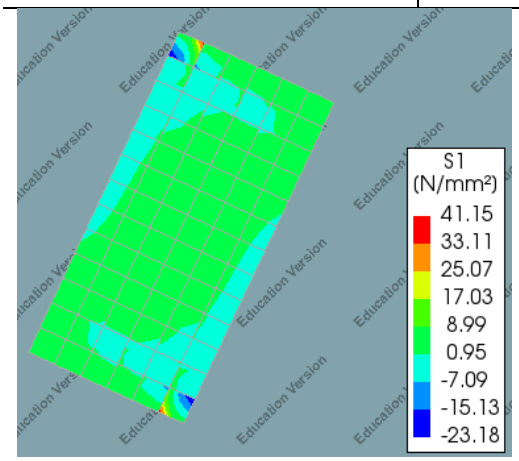	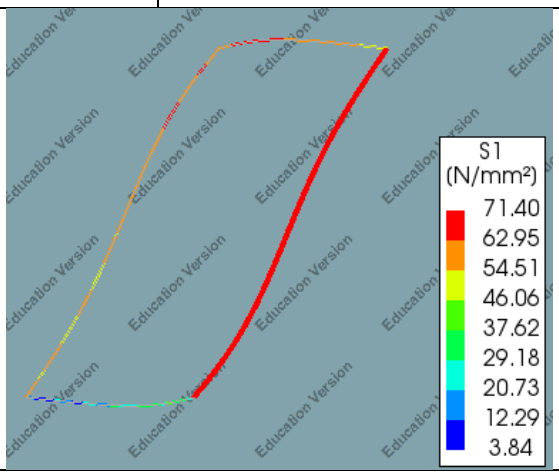	
Total displacement 33 mm		

Table 9: Computational results of a mesh of 100 mm

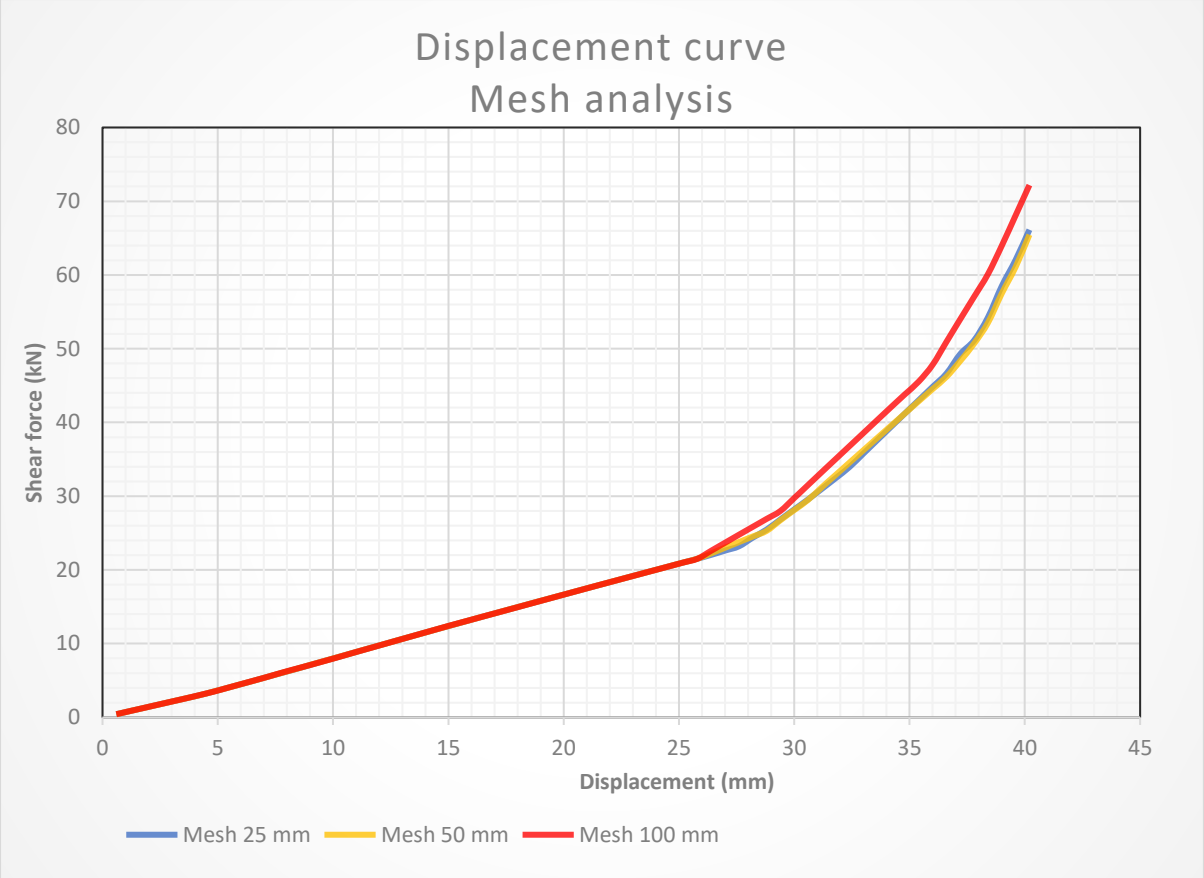

Figure 5: Displacement curve mesh analysis

A.4 Buckling analysis

$$t_{eq,w} = \sqrt[3]{2 * t_{glass}^3 + 12 * I' * J_s}$$

The following information is based on the dimensions of the façade and the properties of the glass.

$E_{glass} = 70{,}000\ MPa$
$b_{glass} = 640\ mm$
$t_{glass,tot} = 20\ mm$
$L_{glass} = 1370\ mm$

t_{int} is the thickness of the interface. In this case, PVB is used with a thickness of 0.38 mm. t_{glass} is the thickness of one glass panel, which has a nominal thickness of 9.7 mm. The initial Shear modulus (G_{int}) is 471 MPa according to the NEN2608. $t_{eq,w}$ is the equivalent thickness according to (Amadio & Bedon, 2015).

$$J_s = \frac{t_{glass}}{2}(t_{glass} + t_{int})^2 = 507.8\ mm^3$$

$$0 \leq I' = \frac{1}{1 + \pi^2 * \beta * \frac{E_{glass} * t_{glass} * t_{int}}{2 * G_{int} * b_{glass}^2}} \leq 1$$

$$I' = 0.95$$

$$t_{eq,w} = \sqrt[3]{2 * t_{glass}^3 + 12 * I' * J_s} = 19.7\ mm$$

The critical shear load is given as $V_{cr}^{(E)}$ for plates that are supported along four sides.

$$V_{cr}^{(E)} = \frac{\pi^2 * D}{b^2} * k_\tau$$

$$D = \frac{E_{glass} * b_{glass} * t_{eq,w}^3}{12(1 - v^2)} = 30{,}156 * 10^6$$

$$a = \frac{L_{glass}}{b_{glass}} = 2.1 > 1$$

$$k_\tau = 5.34 + \frac{4}{a^2} = 6.2\ (hinged\ connection)$$

$$k_\tau = 8.98 + \frac{5.60}{a^2} = 10.2\ (clamped\ connection)$$

$V_{cr}^{(E)} = 4515\ kN(\ hinged)$
$V_{cr}^{(E)} = 7413\ kN\ (rigid)$

The design shear load should be smaller than the bearing resistance of the shear load. The following calculations are assumed for a hinged connection.

$$\lambda_{rel} = \sqrt{\frac{A * \tau_{Rk}}{V_{cr}^{E}}} = \ 0.35$$

The buckling reduction factors take into account the calibrated imperfection and the initial geometrical imperfections.

$a_{imp} = 0.49; \ \ a_0 = 0.50$

$$\emptyset = 0{,}5 * \left[1 + a_{imp}(\lambda_{rel} - a_0) + \lambda_{rel}^2\right] = 0.53$$

$$\chi = \frac{1}{\emptyset + \sqrt{\emptyset^2 - \lambda_{rel}^2}} = 1.09 \ \leq 1 \rightarrow So \ \chi = 1$$

$$V_{ed} \leq V_{b,Rd} = \chi * \frac{A * \tau_{Rk}}{\gamma_m} \ = 405.3 \ kN$$

Thus the bearing resistance of the shear load is 405.3 kN

B. Experimental Research

B.1 Calculation material properties timber

Average density

The surface of the Okoume Multiplex is:

$$A, Ok = 40 * 40 = 1600\ mm^2$$

The surface of the Meranti Wood is:

$$A, Me = 2 * 65 * 30 = 3900\ mm^2$$

Therefore, the average density of the timber frame is:

$$\mathrm{p} = \frac{A, Ok * \mathrm{p, Ok} + \mathrm{A, Me} * \mathrm{p, Me}}{A, tot} = \frac{1600 * \frac{473.4 + 484.90}{2} + 3900 * 601.9}{5500} = 566\ kg/m^3$$

Average Elasticity Modulus

Meranti	Okoume
$E_1 = E_3 = 16.000\ MPa$	$E_2 = 2000\ MPa$ (Old value is 5 GPa)
$h_1 = h_3 = 65\ mm$	$h_2 = 40\ mm$
$b_1 = b_3 = 30\ mm$	$b_2 = 40\ mm$
$I_1 = I_3 = \frac{1}{12} * b * h^3 = 686{,}563\ mm^4$	$I_2 = 213{,}333\ mm^4$

$\gamma_1 = \gamma_2 = \gamma_3 = 1$ ($Glued\ connection$)

$$a_x = \frac{2 * (\gamma_1 * E_1 * A_1 * \left(\frac{h_1}{2}\right)) + \gamma_3 * E_3 * A_3 * \left(\frac{h_2}{2}\right)}{\sum_{i=1}^{3} \gamma_i * E_i * A_i} = 30.96\ mm$$

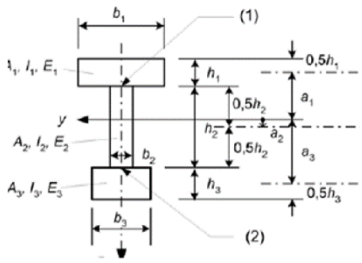

$$a_1 = a_3 = \frac{h_1}{2} - a_x = 1.55\ mm$$

$$a_2 = \frac{h_2}{2} - a_x = -10.96\ mm$$

$$EI_{eff} = \sum_{i=1}^{3} (E_i * I_i + \gamma_i * E_i * A_i * a_i^2) = 24{,}348 * 10^6 Nmm^2$$

$$I_{tot} = I_1 + a_1^2 + I_2 + A_2 * a_2^2 + I_3 + A_3 * a_3^2 = 1814 * 10^3 mm^4$$

$E_{eff} = \frac{EI_{eff}}{I_{tot}} = 12{,}608\ N/mm^2$, This is the stiffness in the bending direction.

B.2 Pre-experiment

To verify the material properties of the used materials a few experiments have been done. The supplier of the Sikaflex-252 adhesive has given the material properties of the adhesive. Furthermore, the properties of the adhesive were also discussed in paragraph 3.1. However, to predict the behaviour of the structural façade the properties of the adhesive still need to be verified. Therefore, a test is done to determine the in-plane shear properties of a timber/glass element bonded by 5 mm thick Sikaflex-252. Specimens were built with black and white Sikaflex-252 by taking samples during the construction of the window. A displacement-controlled procedure was used to evaluate the residual strength properties under precompression. Since there is only done four experiments, no conclusions can be made from these experiments. See Figure 6 for the experimental setup.

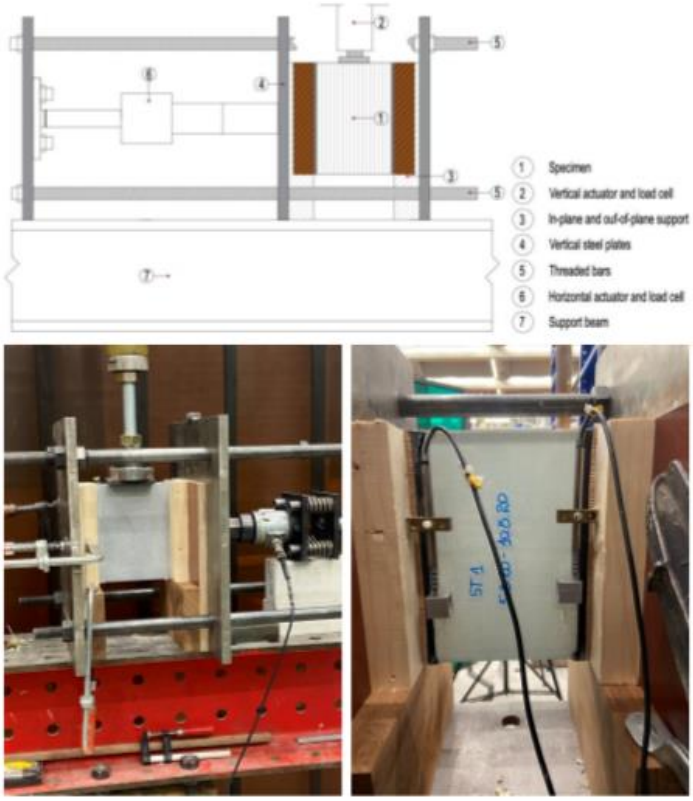

Figure 6: top- drawing of the set-up, left- front side of the specimen with the DIC pattern, right – back of the specimen with sensors applied (Gaggero, 2020)

In Figure 7 the shear stress versus the relative displacement of the glass element for the wooden element is shown. It is shown that the Black Sikaflex has an initial shear stress of approximately 2.1 MPa for a relative displacement of approximately 18 mm. While the White Sikaflex has an initial shear stress of approximately 1.23 MPa for a relative displacement of approximately 12 mm. This difference is not mentioned by the manufacture however, the amount of test is very low to draw any conclusions. Since the manufactures also mention 2 Mpa. It will be concluded that both adhesives behave similarly.

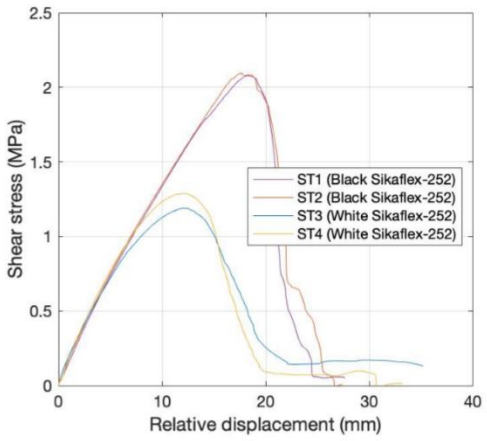

Figure 7: Shear stress versus the relative displacement (Gaggero, 2020)

The amount of pre-compression didn't have a significant influence. See Table 10 for an overview of the properties. See (Gaggero,2020) for more detailed information about the experiment.

Specimen name	f_p (MPa)	f_v (MPa)	$f_{v,res}$ (MPa)	G_{II}(N/mm)
ST1	0.50	2.08	0.07	26.81
ST2	1.00	2.10	-	30.50
ST3	1.00	1.19	0.18	12.09
ST4	0.5	1.29	0.08	14.26

Table 10: Overview of the evaluated properties (Gaggero,2020)

Non-destructive resonance test

The material properties of the timber elements are given by the supplier however, these properties must be verified by experimental results. Therefore, the density and elasticity modulus are determined for both the multiplex and the hardwood element. For the multiplex element “Okoumé” is used and for the hardwood ‘Meranti” is used, see Figure 8. For the Okoumé an additional compression test is done since it will be compressed by the glass element.

Figure 8: left - Okoume Multiplex, right - Meranti Hardwood (Gaggero, 2020)

A non-destructive resonance method has been used to determine the modulus of elasticity by measuring resonance frequencies of vibrations. Sound waves were sent by using a hammer through the wood specimen. See Figure 9. See(M.B.Gaggero, 2020) for further details about the experiment. In Table 11 an overview of the results is given. However, the stiffness for the Okoumé Multiplex is taken to favourable.

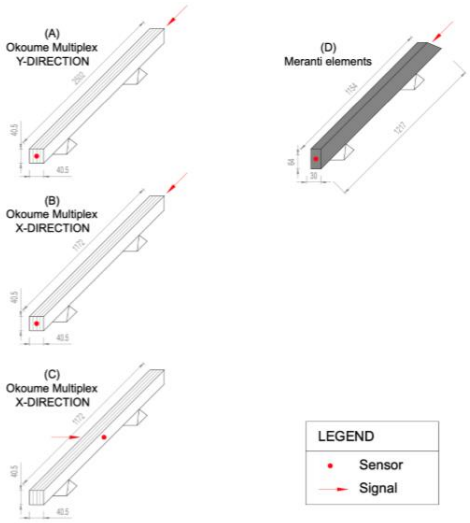

Figure 9: Overview specimens (Gaggero, 2020)

	(A) Okoumé Multiplex Y-Direction	(B) Okoumé Multiplex X-Direction	(D) Meranti elements
L(mm)	2.5020	1.1720	1.1855
B(MM)	0.0405	0.0405	0.0300
H(mm)	0.0405	0.0405	0.0640
V(mm^3)	0.0041	0.0019	0.0023
W(kg)	1.99	0.91	1.37
f(Hz)	1425	683	2176
$\boldsymbol{p\ (kg/mm^3)}$	**473.4**	**484.9**	**601.9**
E (GPa)	**5.7**	**5.3**	**16.0**

Table 11: Overview results (Gaggero, 2020)

According to the experiment the average stiffness is 5.5 GPa however, the supplier mentioned a bending stiffness of 2 GPa. Therefore, further research was needed. A compression test is done to measure the bending stiffness and the compression strength of the plywood. In Table 13 the results of the compression test for the Okoumé are shown. An average bending stiffness of 1.63 GPa is given. This proves that the former average stiffness of 5.5 GPa is taken to favourably. Since the supplier mentioned a bending stiffness of 2 GPa, this will value will be used for the calculation for average elasticity modulus. In the previous paragraphs, a value of 5.5 GPa is taken for the numerical models. Since the main point was to compare the models these values are not adjusted. However in the next paragraphs, the value of 2 GPa is assumed for the plywood. The calculation includes the estimated average density and elasticity modulus of the composed timber frame. This is of importance since this will be the input value of the computational model. See Appendix B.1 for the calculation and Table 12 for the new value for the timber frame.

	Calculated	Input for model
Average density (kg/m^3)	566	565
Average Elasticity Modulus (N/mm^2)	12,608	12,500

Table 12: Timber material properties

Compression test

The compression test of the Okoumé Multiplex is done with a specimen of 40 mm *40 mm *40 mm. This was done because stability problems occurred with slender profiles. In total 5 specimens are tested. The results of the compression test are given in Table 13 and Figure 10. These results will be used as input values for the numerical model.

Specimen	$f_{c,y}$ (MPa)	$f_{c,u}$ (Mpa)	$E_c\ (GPa)$
A	13.4	23.18	1.83
B	12.50	22.26	1.85
C	12.77	22.81	1.81
D	13.87	22.72	1.49
E	12.68	22.36	1.63
Avg.	12.99	22.66	**1.63**
St.dev.	0.54	0.37	0.16
C.o.V	0.04	0.02	0.09
Characterisitc value	**11.66**	**21.76**	-

Table 13: Compression test results

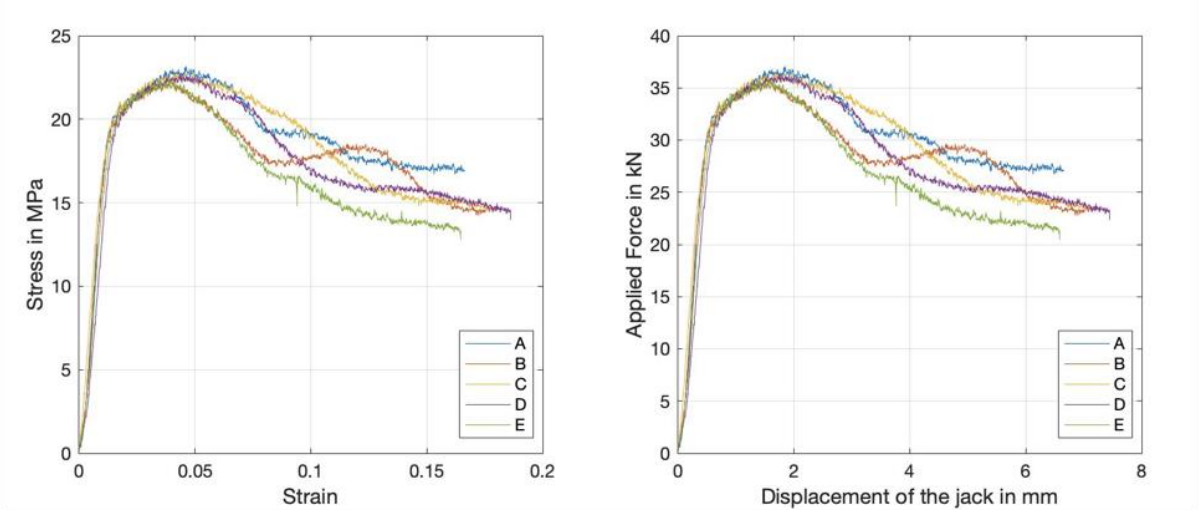

Figure 10: left – stress-strain curve, right- displacement versus applied force

These results are significantly higher than what the supplier advised as the compression strength. For the Okoume multiplex, the supplier advised a characteristic class of F15/20 for strength in bending, tension and compression for a thickness of 40 mm. The characteristic class for stiffness in bending and tension-compression for a thickness of 40 mm is E35/40. See Table 14 and Table 15 and Figure 11. This comes down to a compression and tension strength of 8 MPa and a bending stiffness of 2 GPa since the timber frame is loaded parallel to the grain.

	Bending $f_m(MPa)$	Compression $f_{c\|\|}$ Tension $f_{t\|\|}$	Compression $f_{c\perp}$ Tension $f_{t\perp}$
F15	15	6	7.5
F20	20	8	10

Table 14: Strength class Multiplex

	Bending E_m (MPa)	Compression $E_{c\|\|}$ Tension $E_{t\|\|}$ (MPa)	Compression $E_{c\perp}$ Tension $E_{t\perp}(MPa)$
E30	3000	1500	2400
E40	4000	2000	3200

Table 15: Class for stiffness of Multiplex

A strength class of F15 gives the following strength values:
Bending $f_m = 15\ MPa$
Compression $f_{c||}$ = Tension $f_{t||} = 6\ MPa$ (Parallel to the grain)
Compression $f_{c\perp}$ = Tension $f_{t\perp} = 7.5\ MPa$ (Perpendicular to the grain)

A strength class of F20 gives the following strength values:
Bending $f_m = 20\ MPa$
Compression $f_{c||}$ = Tension $f_{t||} = 8\ MPa$ (Parallel to the grain)
Compression $f_{c\perp}$ = Tension $f_{t\perp} = 10\ MPa$ (Perpendicular to the grain)

The modulus of elasticity of E30 gives the following stiffness values:
Bending $E_m = 3000\ MPa$
Compression $E_{c||}$ = Tension $fE_{t||} = 1500\ MPa$ (Parallel to the grain)
Compression $E_{c\perp}$ = Tension $E_{t\perp} = 2400\ MPa$ (Perpendicular to the grain)

The modulus of elasticity of E40 gives the following stiffness values:
Bending $f_m = 4000\ MPa$
Compression $E_{c||}$ = Tension $E_{t||} = 2000\ MPa$ (Parallel to the grain)
Compression $E_{c\perp}$ = Tension $E_{t\perp} = 3200\ MPa$ (Perpendicular to the grain)

Class for stiffness [2]	Mean modulus (MPa) [3]		
	Surface grain direction [2]		
	0 and 90	0	90
	Bending E_m	Tension E_t Compression E_c	
E5	500	250	400
E10	1 000	500	800
E15	1 500	750	1 200
E20	2 000	1 000	1 600
E25	2 500	1 250	2 000
E30	3 000	1 500	2 400
E40	4 000	2 000	3 200
E50	5 000	2 500	4 000
E60	6 000	3 000	4 800
E70	7 000	3 500	5 600
E80	8 000	4 000	6 400
E90	9 000	4 500	7 200
E100	10 000	5 000	8 000
E120	12 000	6 000	9 600
E140	14 000	7 000	11 200

Strength class [2]	Characteristic strength values (MPa)		
	Surface grain direction [2]		
	0 and 90	0	90
	Bending f_m	Tension f_t Compression f_c	
F3	3	1,2	1,5
F5	5	2	2,5
F10	10	4	5
F15	15	6	7,5
F20	20	8	10
F25	25	10	12,5
F30	30	12	15
F40	40	16	20
F50	50	20	25
F60	60	24	30
F70	70	28	35
F80	80	32	40

Figure 11: Left: Classification for modulus of elasticity of plywood in bending, compression and tension
Right: Characteristic strength values of plywood, to be used in structural design ("Design of timber structures," 2016)

C. Numerical model Optimised

C.1 Calculation equivalent stiffness

$$k = \frac{F}{u} \rightarrow\ k_1 = \frac{\sigma_1}{u_1}\ ; k_2 = \frac{\sigma_2}{u_2}\ ;$$

$$\frac{1}{k_{eq}} = \frac{1}{k_1} + \frac{1}{k_2}$$

$$\sigma_{eq} = k_{eq} * (u_1 + u_{2)}$$

The interface is modelled as a serial system of 2 springs, the adhesive and the multiplex. For tension forces, the same stiffness properties are assumed as for the adhesive. The multiplex has a significantly low contribution to the stiffness for tension since the adhesive is significantly stiffer in tension.

In order to add the stiffness of the serial system to each other, the forces or stresses need to be the same. The calculation of the serial spring system for a total displacement of -6.67 mm is shown below.

$$k = \frac{F}{u} \rightarrow\ k_1 = \frac{\sigma_1}{u_1}\ ; k_2 = \frac{\sigma_2}{u_2}\ ;$$

$k_1 = \frac{-22.5}{-5.07} = 4.4\ N/mm^3$; $\quad k_2 = \frac{-22.5}{-1.6} = 14.1 N/mm^3$

$u_{tot} = -5.07 - 1.6 = -6.67\ mm$; $\quad \frac{1}{k_{eq}} = \frac{1}{4.4} + \frac{1}{14.1} \rightarrow\ k_{eq} = 3.37\ N/mm^3$

$\sigma_{eq} = 3.37 * -6.67 = -22.5\ N/mm^2$

After the total displacement of -6.67 mm the stiffness of the multiplex decreases, while the stiffness of the adhesive increases. As mentioned before, the forces need to be the same in both springs. Therefore, the force in both springs decrease. The compression force of the multiplex for a displacement of -6 mm is -15 N/mm^2. The adhesive has a displacement of -4.25 mm for a compression force of -15 N/mm^2. Therefore, the total displacement is -10.25 mm for this compression force. Since the compression force doesn't change significantly by increasing the displacement. The equivalent compression force remains the same while the displacement increases, see Table 16.

Serial spring system								
Adhesive stiffness properties			Timber stiffness properties			Equivalent stiffness		
u_1 (mm)	σ_1 (N/mm^2)	k_1 (N/mm^3)	u_2 (mm)	σ_2 (N/mm^2)	k_2 (N/mm^3)	u_{tot} (mm)	k_{eq} (N/mm^3)	σ_{eq} (N/mm^2)
-25	-1200	48	-	-15	-	-25	-	-15
-10	-1200	120.0	-	-15	-	-	-	-15
-8	-689	86.1	-	-15	-	-	-	-15
-5.5	-50	9.1	-	-15	-	-10.25	-	-15
-5.07	-22.5	4.4	-1,6	-22,5	14,1	-6.67	3.37	-22.50
-5	-18	3.6	-0,5	-18	36.0	-5.5	3.27	-18.00
-0.75	-0.9	1.2	-0,024	-0.9	41.7	-0.774	1.17	-0.90
0	0	0.0	0	0	0	0	0	0
0.75	0.9	1.2	-	-	-	0.75	1.2	0.9
2.50	1	0.4	-	-	-	2.5	0.4	1
25	0.001	$4 * 10^{-5}$	-	-	-	25	$4 * 10^{-5}$	0.001

Table 16: Overview of the stiffness properties

C.2 Overview phases – Adjusted numerical model

Relative Interface Displacement	Maximum Stress Glass
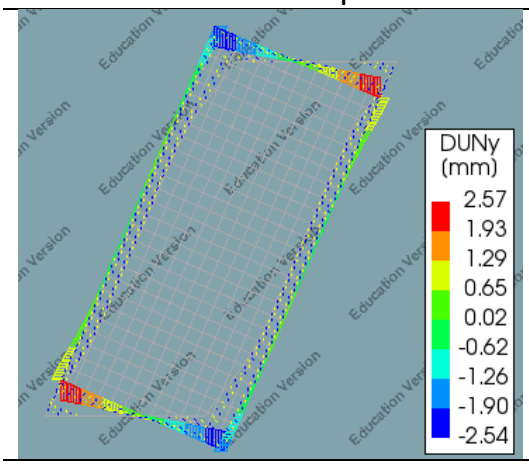	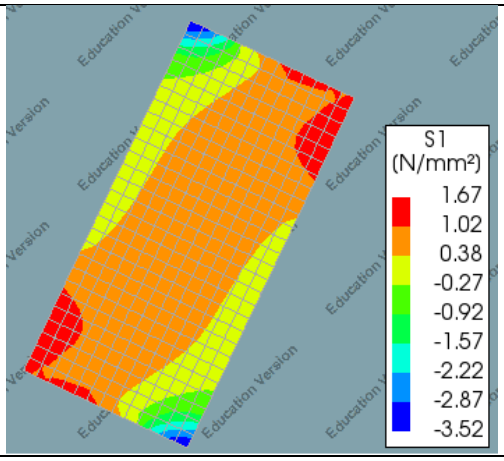
Total Displacement: 14 mm Relative Interface displacement: +2,5 mm	
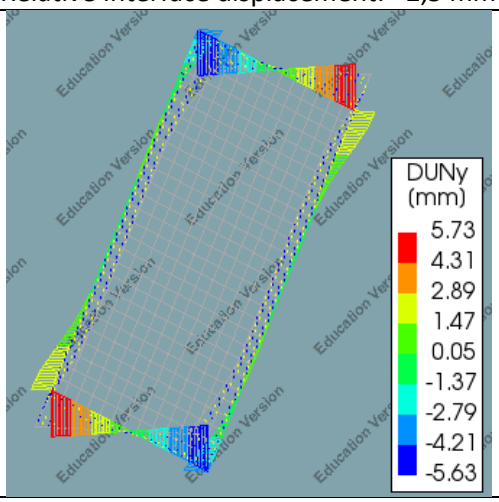	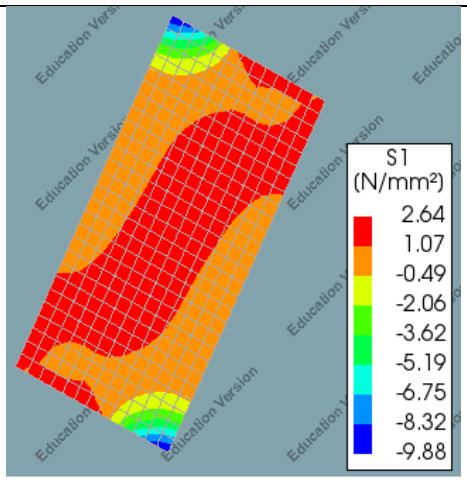
Total Displacement: 31 mm Relative Interface Displacement-5,5 mm	
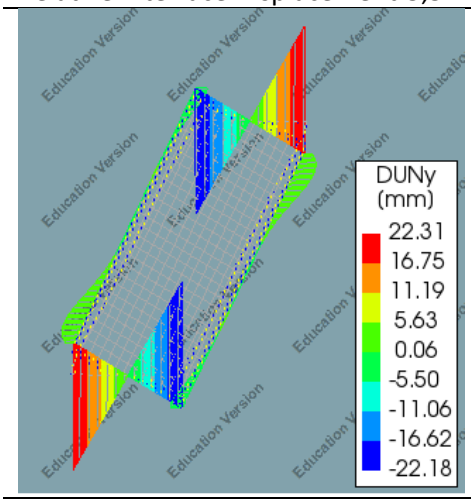	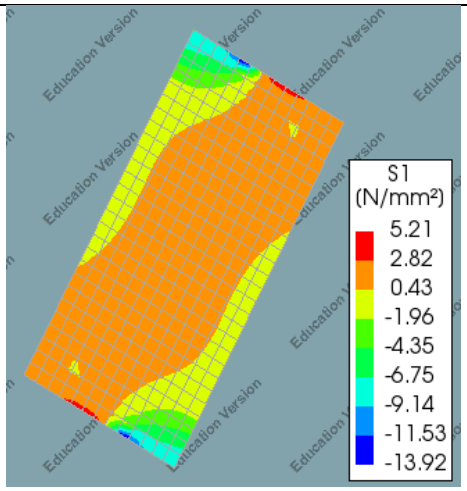
Total Displacement: 100 mm	Maximum stress: + 5 Mpa

Table 17: Overview stresses and relative interface for the adjusted numerical model for the structural window frame

C.3 Overview of relative interface displacement between numerical model and experiment

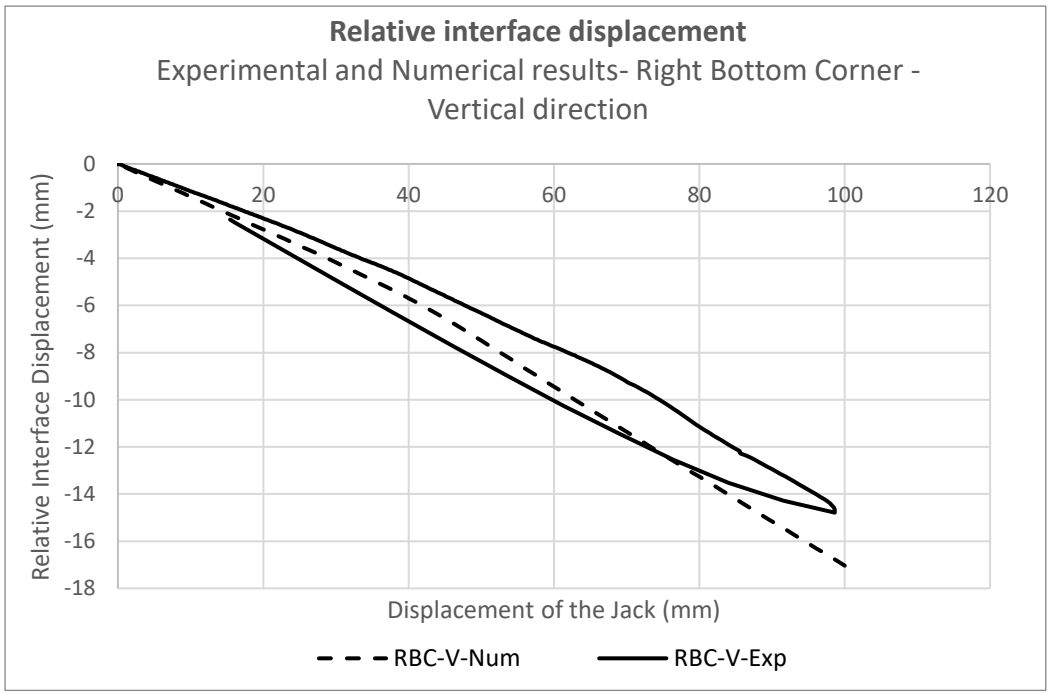

Figure 12: Relative interface displacement of the numerical model and the experiment for the right bottom corner

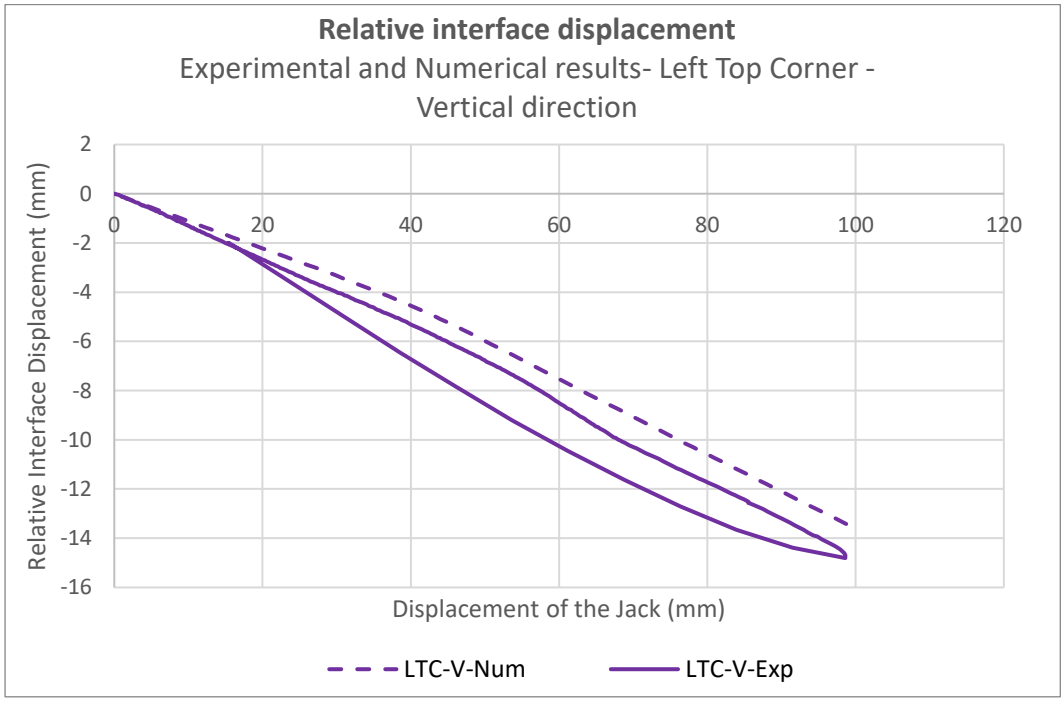

Figure 13: Relative interface displacement of the numerical model and the experiment for the left top corner

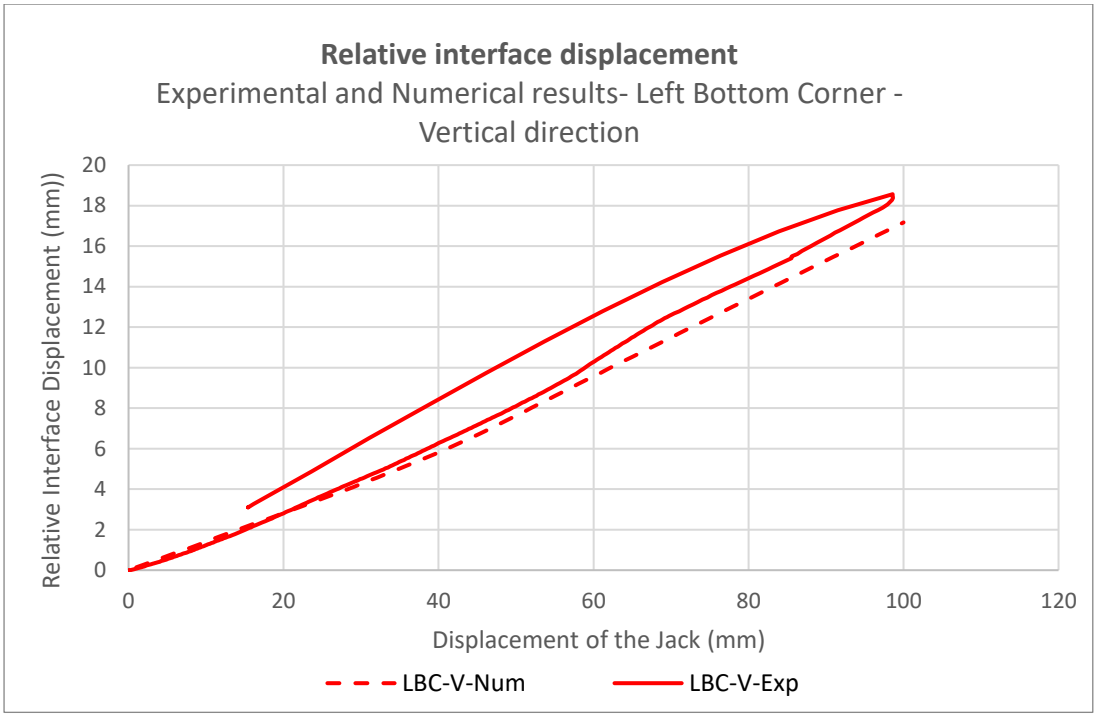

Figure 14: Relative interface displacement of the numerical model and the experiment for the left bottom corner

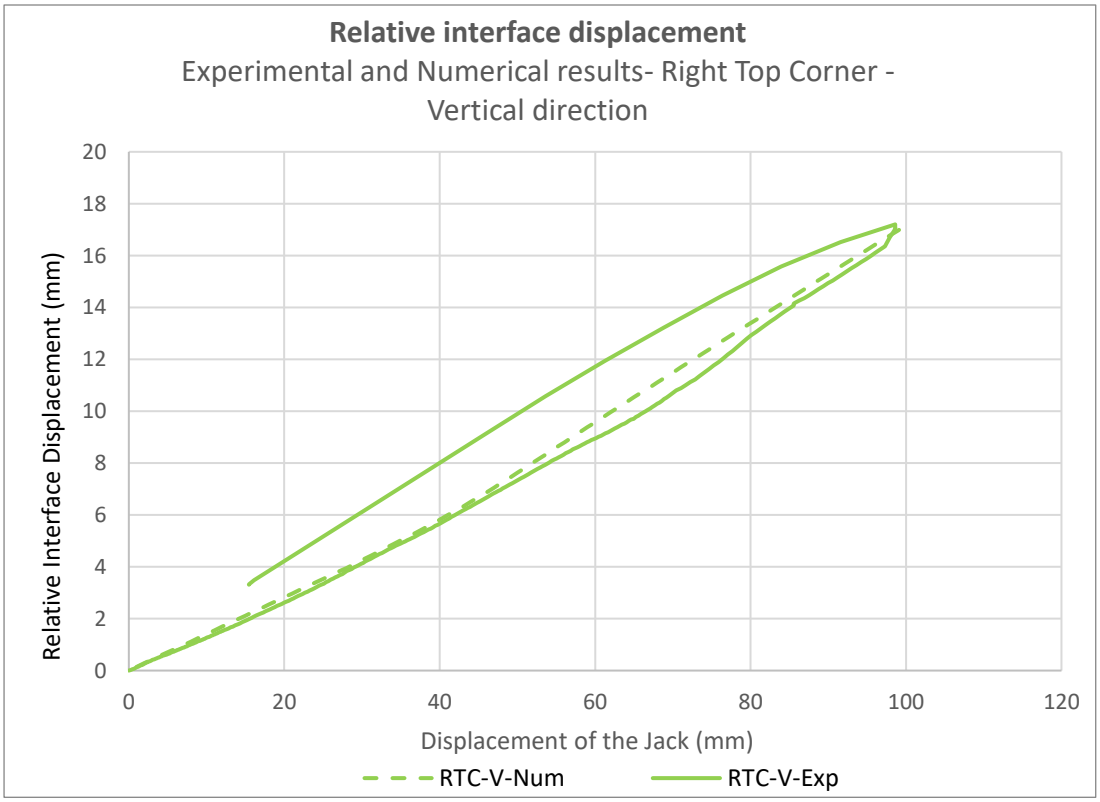

Figure 15: Relative interface displacement of the numerical model and the experiment for the right top corner

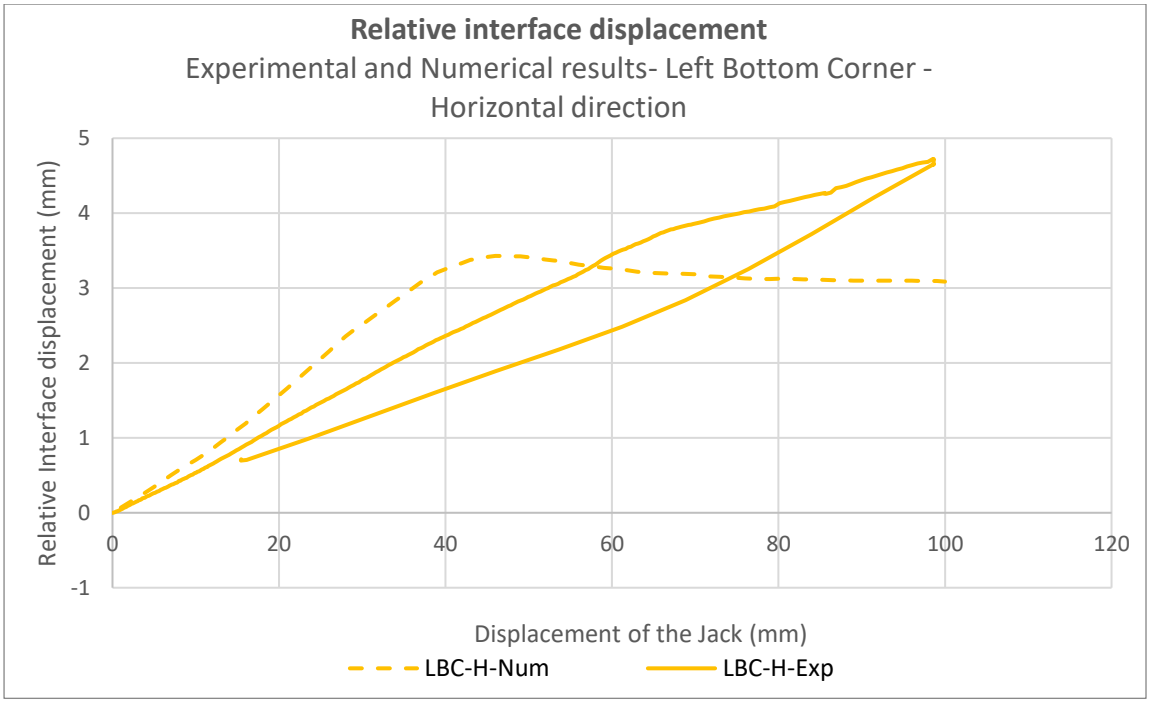

Figure 16: Relative interface displacement of the numerical model and the experiment for the left bottom corner

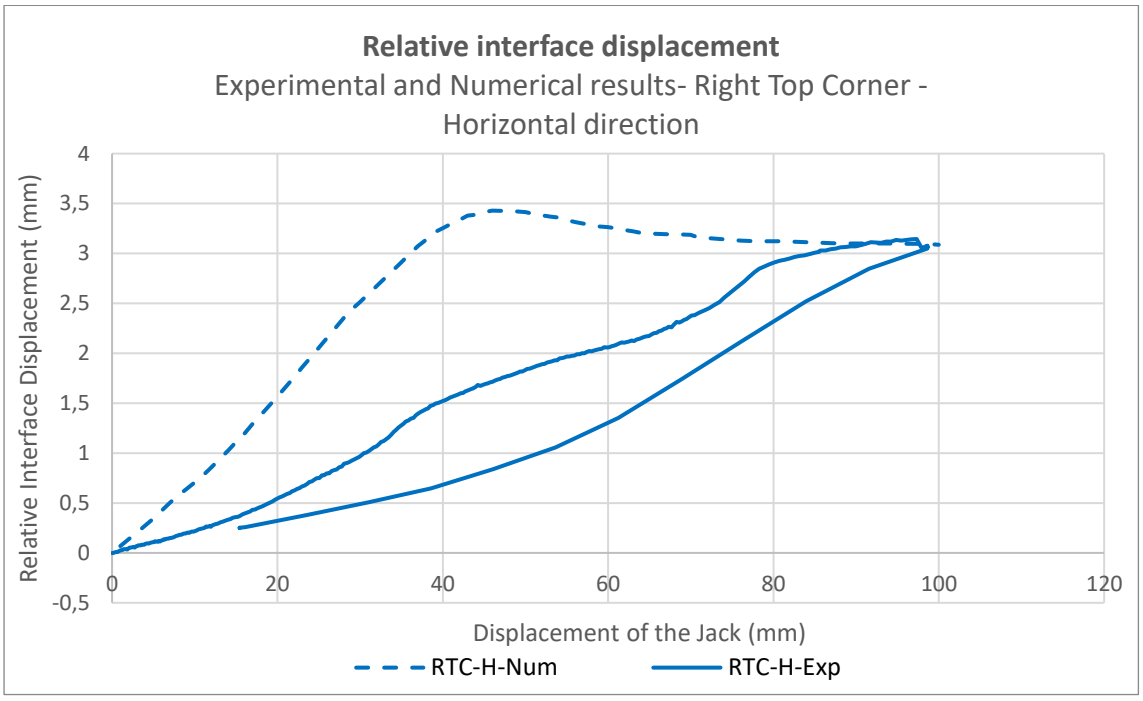

Figure 17: Relative interface displacement of the numerical model and the experiment for the right top corner

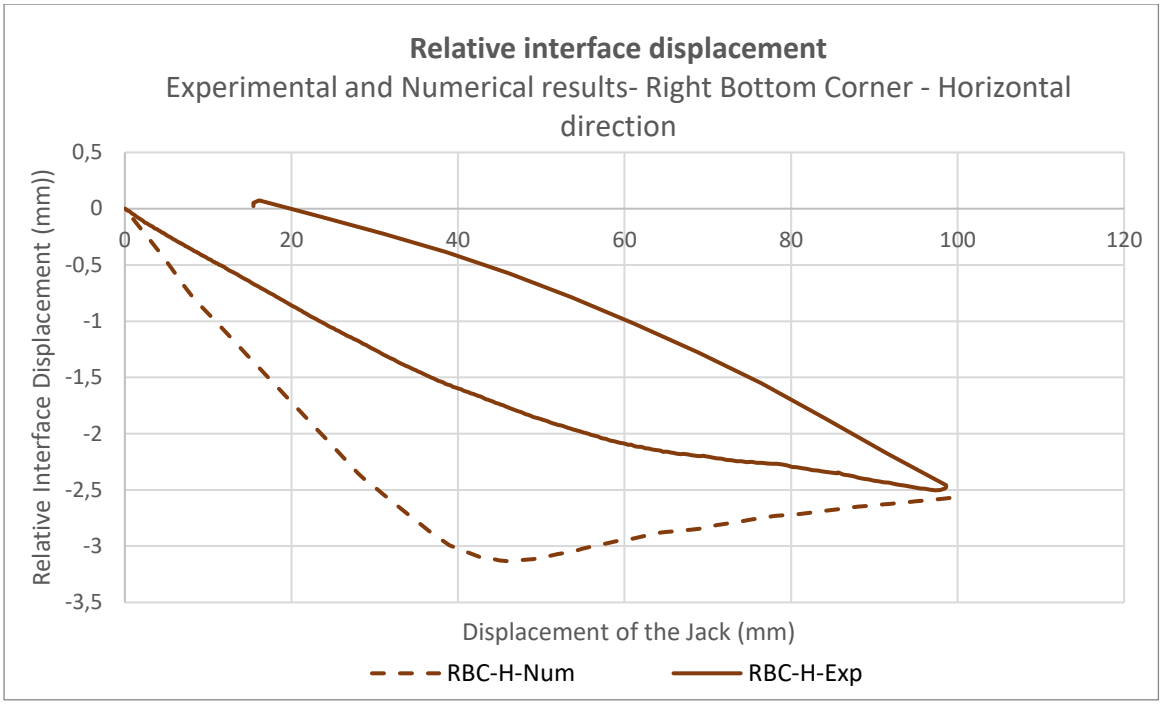

Figure 18: Relative interface displacement of the numerical model and the experiment for the right bottom corner

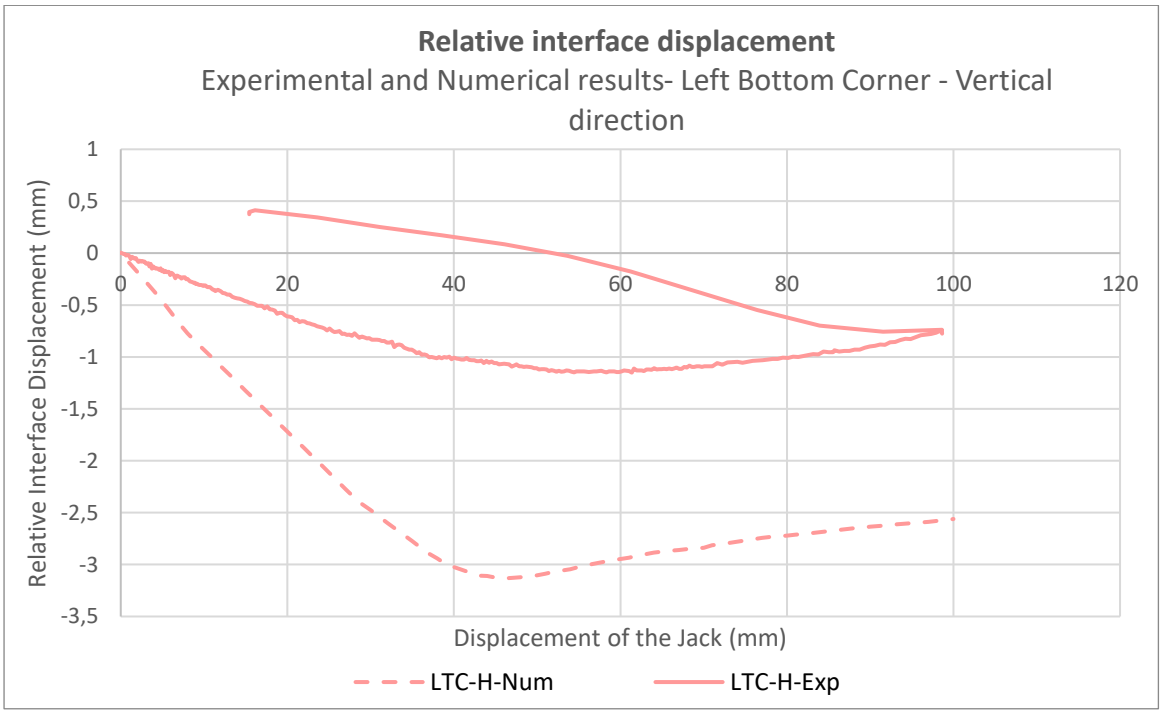

Figure 19: Relative interface displacement of the numerical model and the experiment for the left top corner

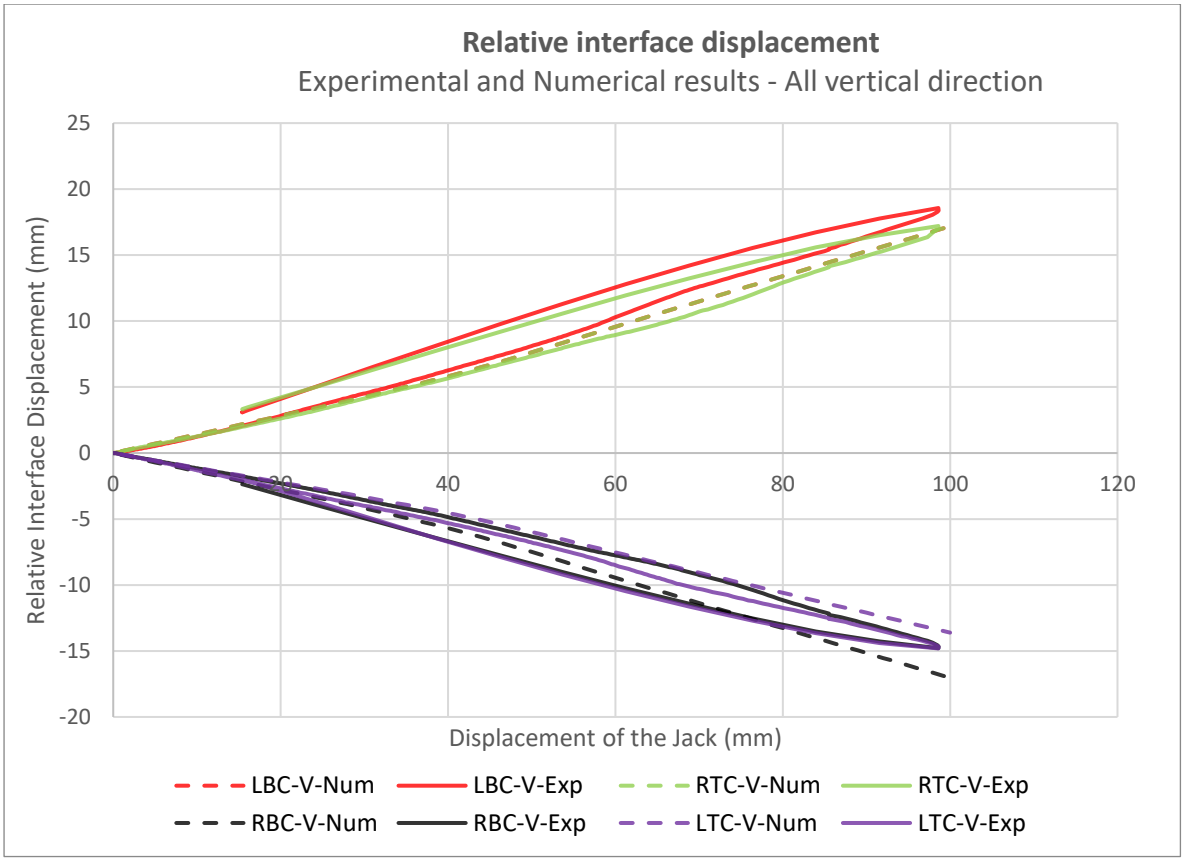

Figure 20: Relative interface displacement of the numerical model and the experiment for all vertical direction

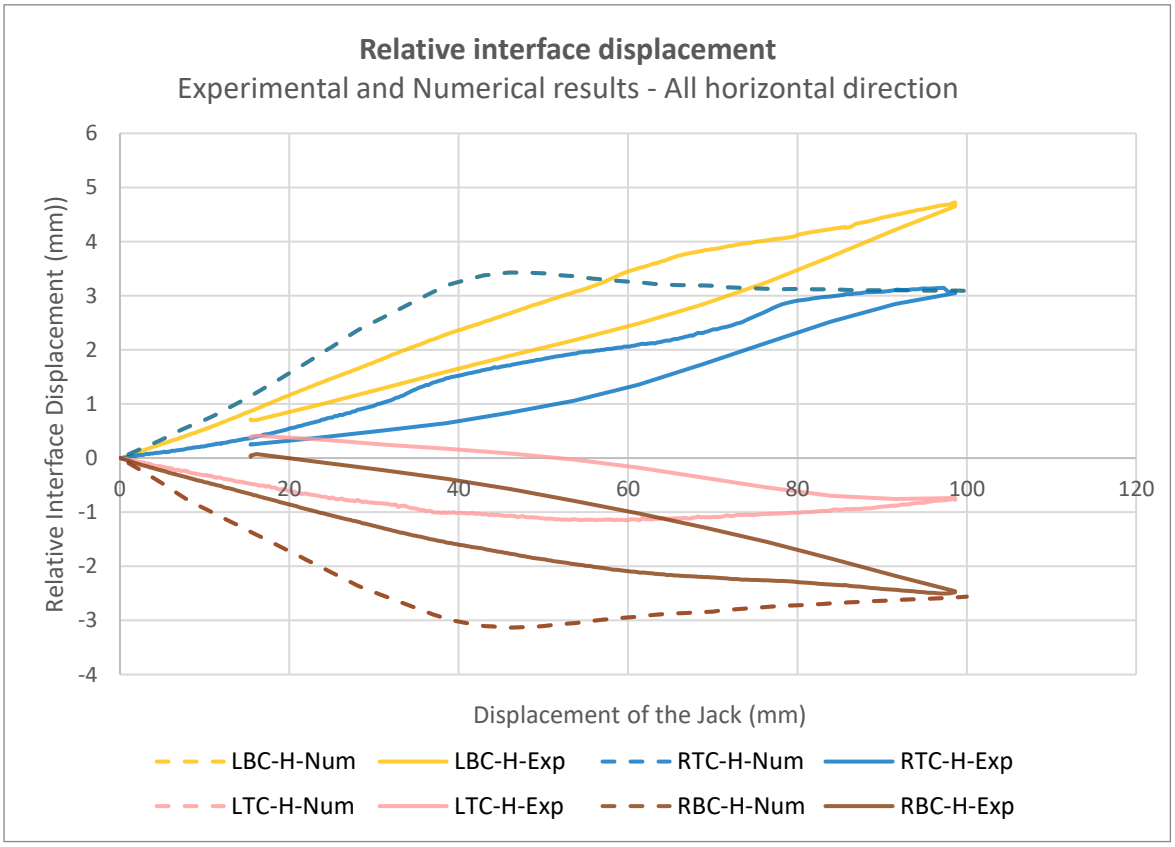

Figure 21: Relative interface displacement of the numerical model and the experiment for all horizontal direction

D. Numerical masonry model

D.1 Overview crack width and stresses

Numerical masonry model 1	Numerical masonry model 2	Numerical masonry model 3
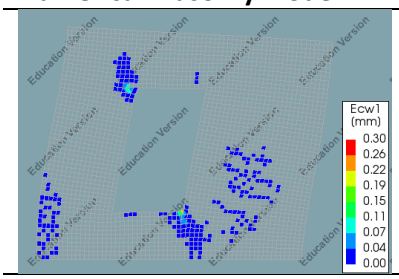	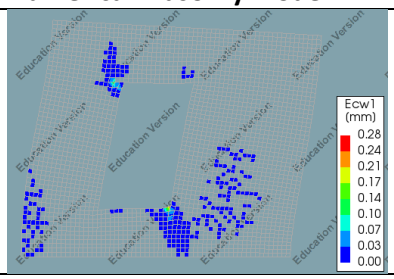	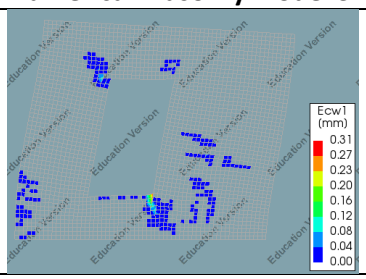
End of the Linear elastic stage Load step 44: 0.69 mm displacement		
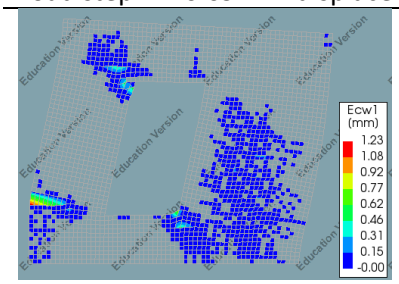	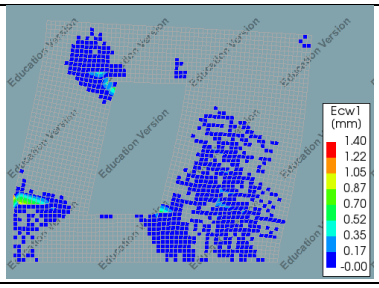	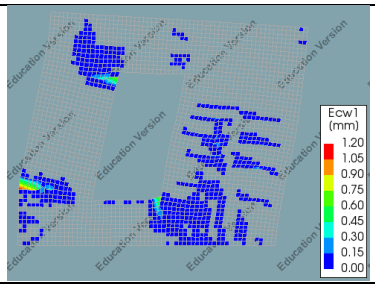
End of the experiment Load step 98: 1.55 mm displacement		
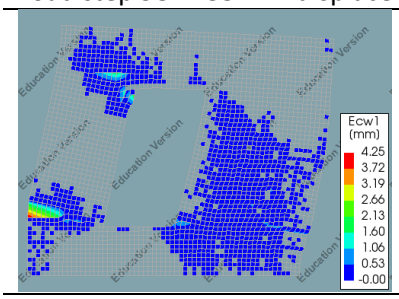	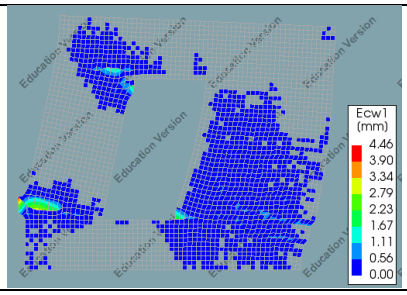	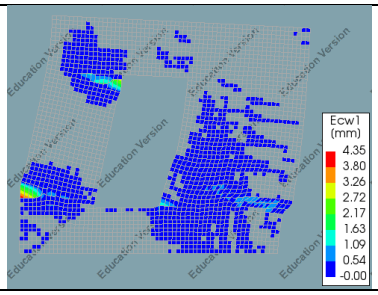
End of the numerical model Load step 250: 4 mm displacement		

Table 18: Overview crack width of numerical masonry model 1,2 & 3

Numerical masonry model 1	Numerical masonry model 2	Numerical masonry model 3
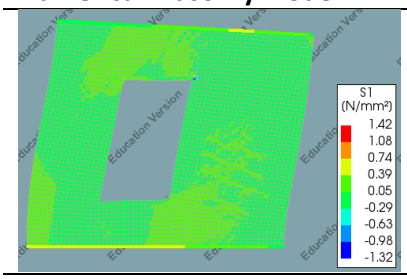	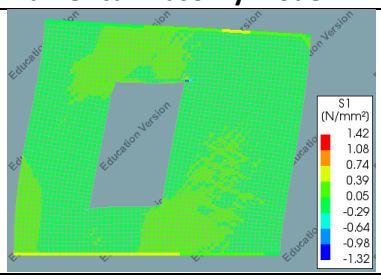	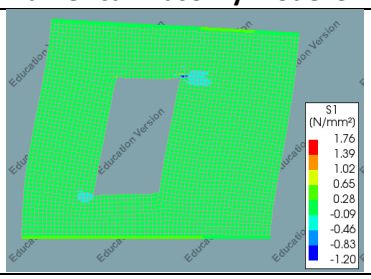
End of the Linear elastic stage Load step 44: 0.69 mm displacement		
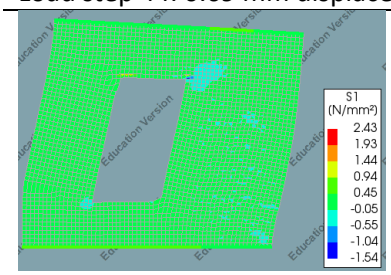	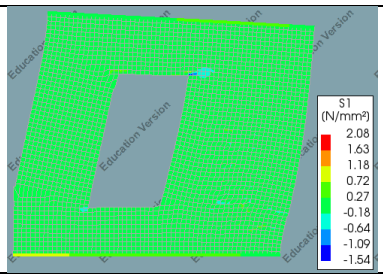	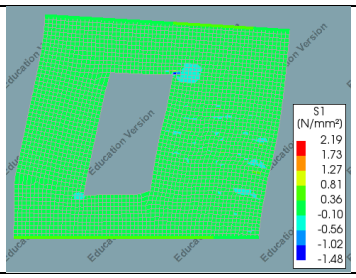
End of the experiment Load step 98: 1.55 mm displacement		
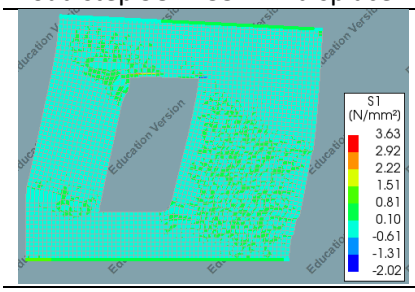	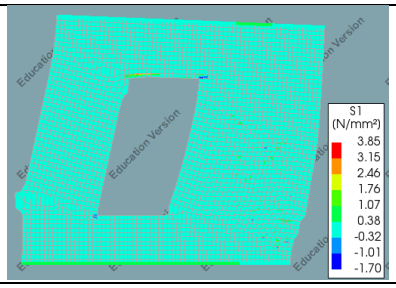	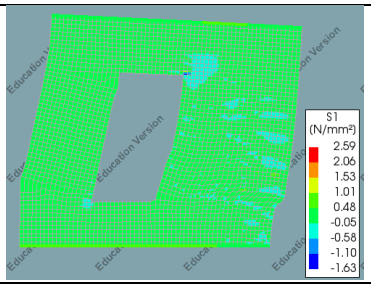
End of the numerical model Load step 250: 4 mm displacement		

Table 19: Overview of stresses for numerical masonry model 1,2 & 3

D.2 Overview of crack propagation for masonry models

Numerical masonry model 2: Original hole	Numerical masonry model 4: Smaller hole
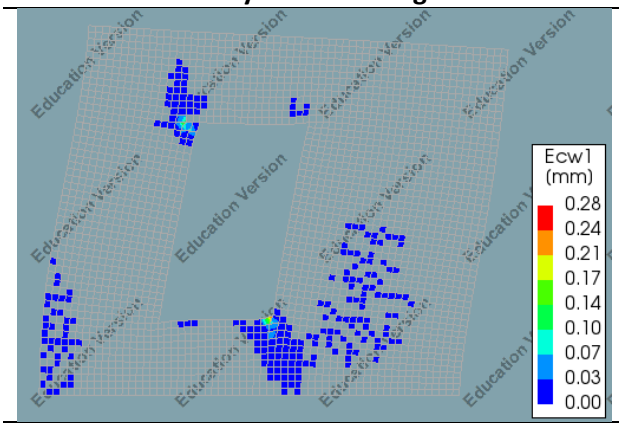	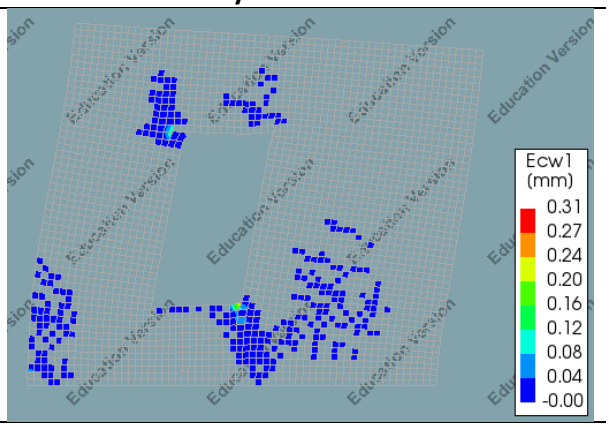
End of the Linear elastic stage Load step 18: 0.68 mm displacement	
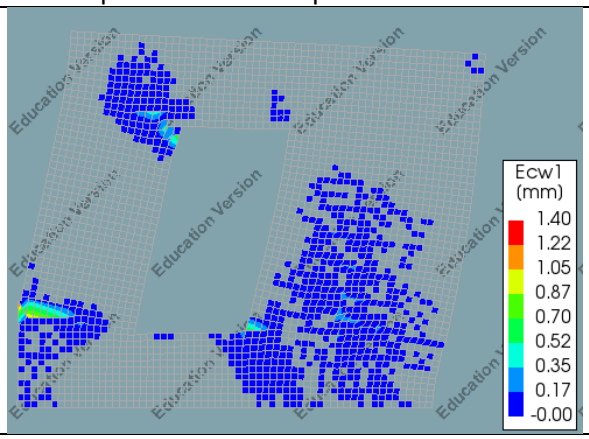	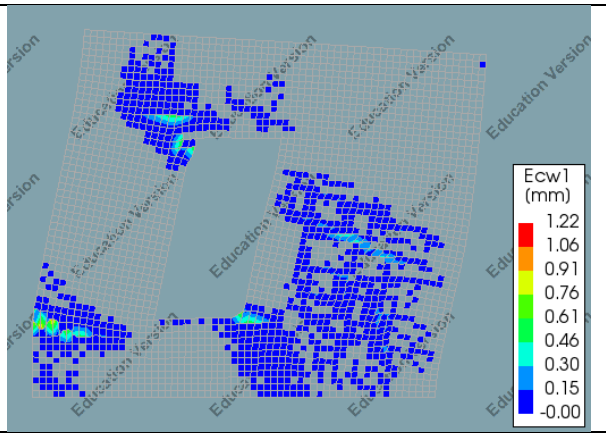
End of the experiment Load step 40: 1.56 mm displacement	
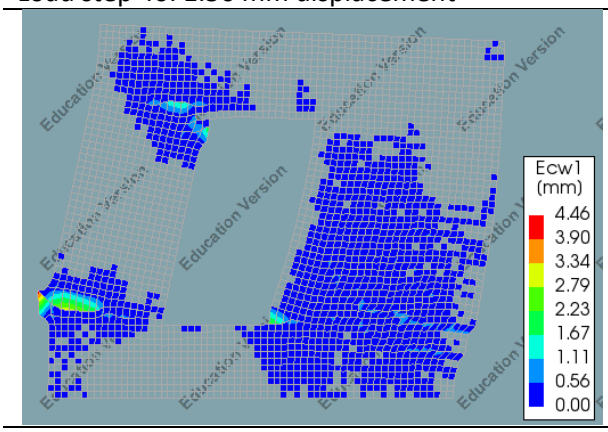	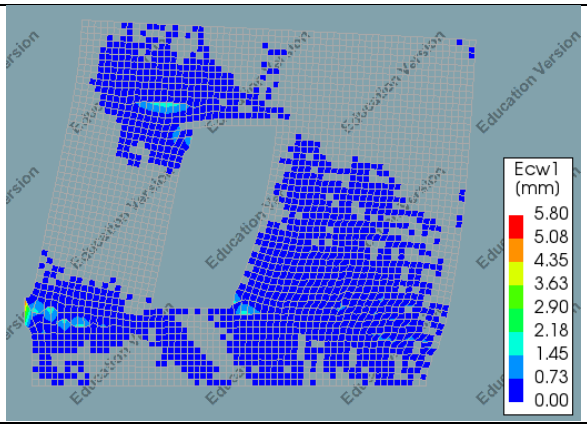
End of the numerical model Load step 100: 4 mm displacement	

Table 20: Overview of the crack propagation for the numerical masonry model 2 & 4

Numerical masonry model 2: Original hole	Numerical masonry model 4: Smaller hole
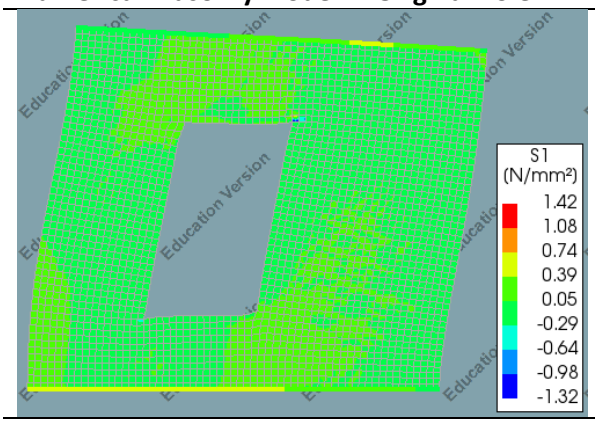	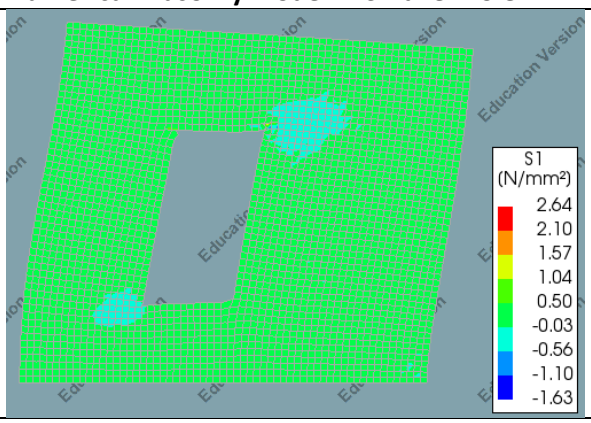
End of the Linear elastic stage Load step 18: 0.68 mm displacement	
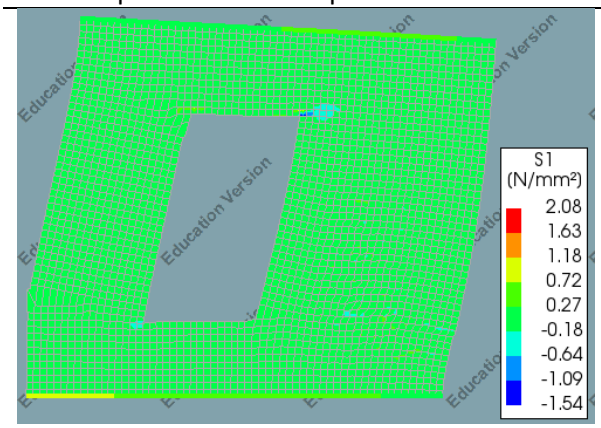	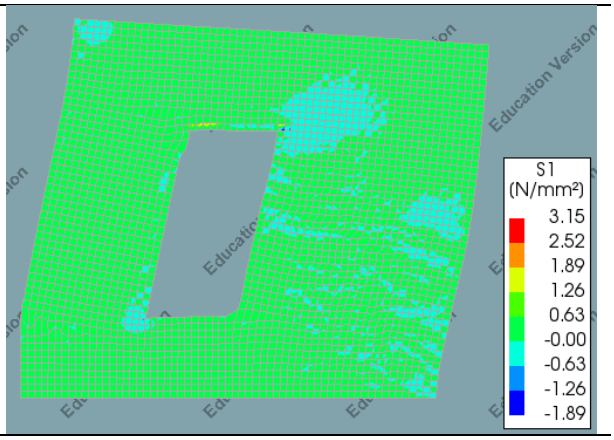
End of the experiment Load step 40: 1.56 mm displacement	
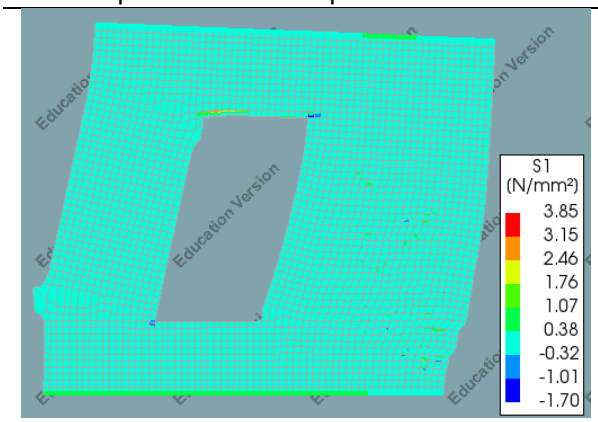	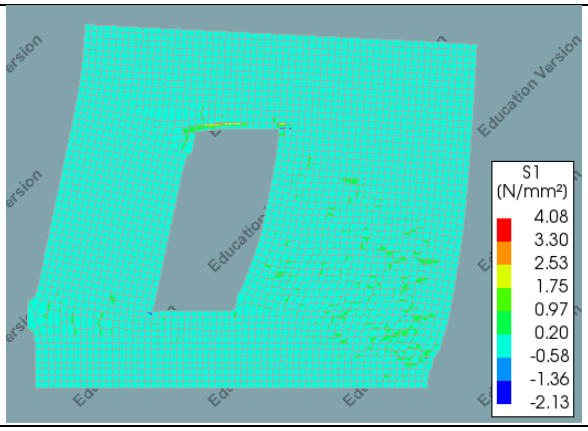
End of the numerical model Load step 100: 4 mm displacement	

Table 21: Overview of the stresses for the numerical masonry model 2 & 4

D.3 Non-linear Pushover calculation

Firstly, the effective mass needs to be calculated, which is the total weight that rests on the masonry wall.

$m_1 = 2400\ kg$

$m_2 = 2400\ kg$

$m_3 = 1200\ kg$

$m_{eff} = 6000\ kg$

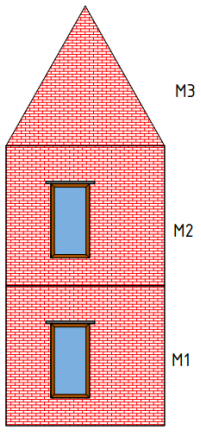

Figure 22: Effective mass

Secondly the total deformation energy (E_m) needs to be calculated. Knowing the deformation energy and the maximum shear force (F_y), leads to calculating the yield displacement($u_{y;sys}$).
E_m = 1211 Nm, See Table 22.

Distance (mm)	Force (kN)	Energy (Nm)
0,7	23,5	8
18	44,5	588
33	37,5	614,6
Total		1211

Table 22: Overview of the total energy in Nm

$u_{cap;sys} = 33\ mm = 0{,}033\ m$ (near collapse displacement capacity)
$F_y = 44\ 500\ N$

$$u_{y;sys} = 2 * \left(u_{cap;sys} - \frac{E_m}{F_y}\right) = 2 * \left(0{,}033 - \frac{1211}{44\ 500}\right) = 0{,}0115\ m = 11{,}5\ mm$$

This gives the following bilinear curve, see Figure 23.

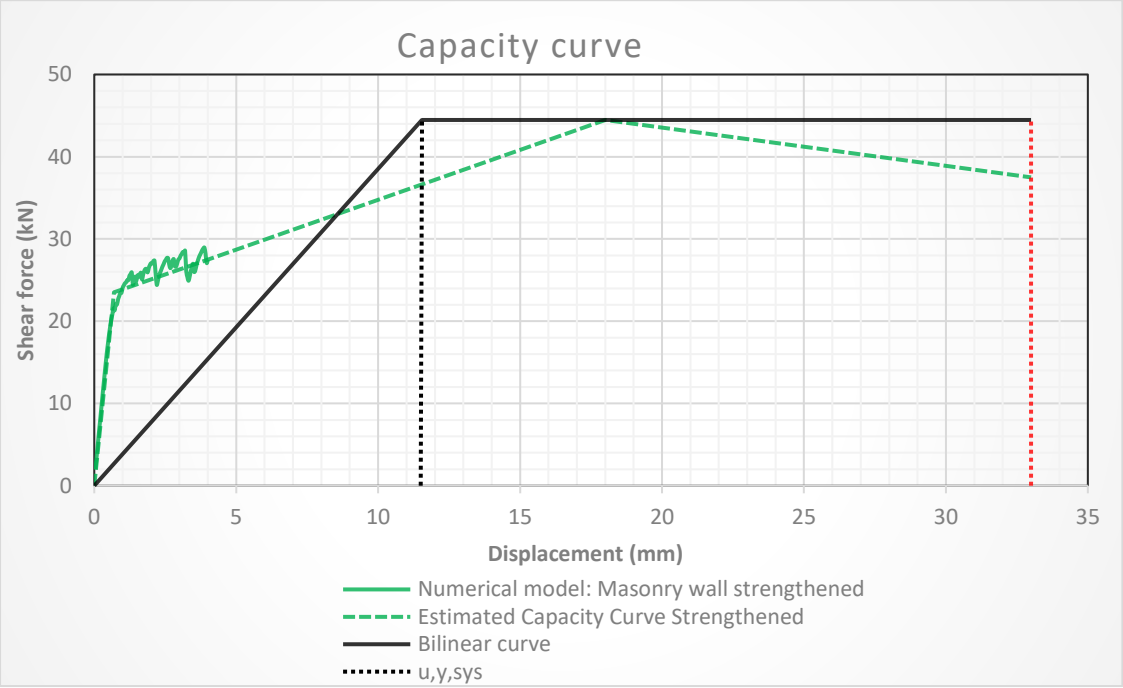

Figure 23: Bilinear capacity curve for the strengthened masonry wall

$$T_* = 2 * \pi * \sqrt{\frac{m_{eff*} u_{y;sys}}{F_y}} = 0{,}25\ s\ \ (Effective\ period)$$

$$u_{sys} = \frac{u_{duc;sys}}{u_{y;sys}} = \frac{33}{11{,}5} = 2{,}9$$

Now the ductility factor (u_{sys}) is known and the damping factor(ε_{sys}) and the spectral reduction factor(η_ε) can be calculated.

$\varepsilon_{sys} = \varepsilon_0 + \varepsilon_{hys} + \beta_0 \leq 0{,}4$ (40%)
$\varepsilon_0 = inherent\ damping \rightarrow 5\%\ for\ unreinforced\ masonry$

$$\varepsilon_{hys} = hysterical\ damping \rightarrow 0{,}42 * \left(1 - \frac{0{,}9}{\sqrt{u_{sys}}} - 0{,}1 * \sqrt{u_{sys}}\right) \leq 0{,}15$$

$$\varepsilon_{hys} = 0{,}42 * \left(1 - \frac{0{,}9}{\sqrt{u_{sys}}} - 0{,}1 * \sqrt{u_{sys}}\right) = 0{,}125 \leq 0{,}15$$

$\beta_0 = the\ effect\ of\ the\ radiation\ demping\ for\ a\ foundation, this\ can\ be\ neglected\ for\ housing\ of\ two\ buildinglayers.$
$\varepsilon_{sys} = 0{,}05 + 0{,}125 + 0 = 0{,}175 = 18\% \leq 0{,}4$

$$\eta_\varepsilon = \sqrt{\frac{7}{2+\varepsilon_{sys}}} = 0{,}60$$

In Figure 24 the ADRS curve of Appingedam and the reduced ADRS curve is shown. The redurced non-linear ADRS curve is not used when ADRS curve intersects with the bilinear curve in the elastic region since damping is than not applicable.

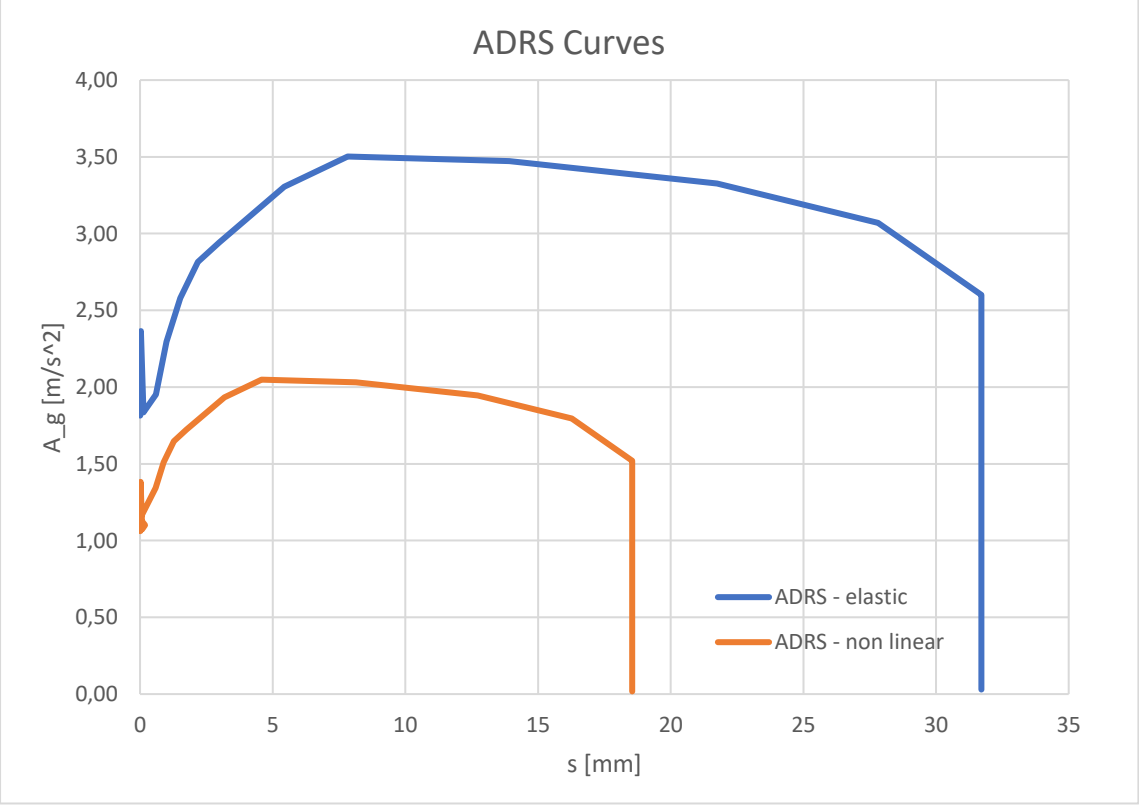

Figure 24: ADRS Curve for Appingedam

In Figure 25 the ADRS curve for the ULS and the SLS are shown. The return period for the ULS is 2475 years and for the SLS is 95 years. This difference is clearly seen in the bottom graph.

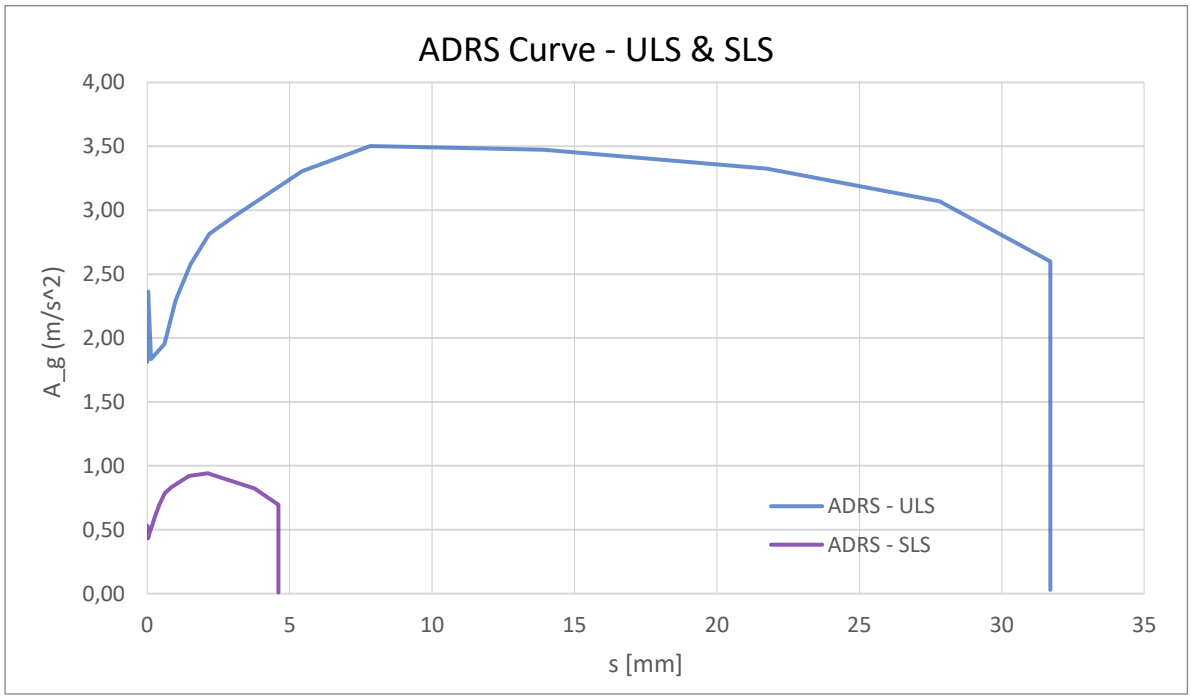

Figure 25: ADRS curve for the ultimate limit stage and the serviceability imit stage

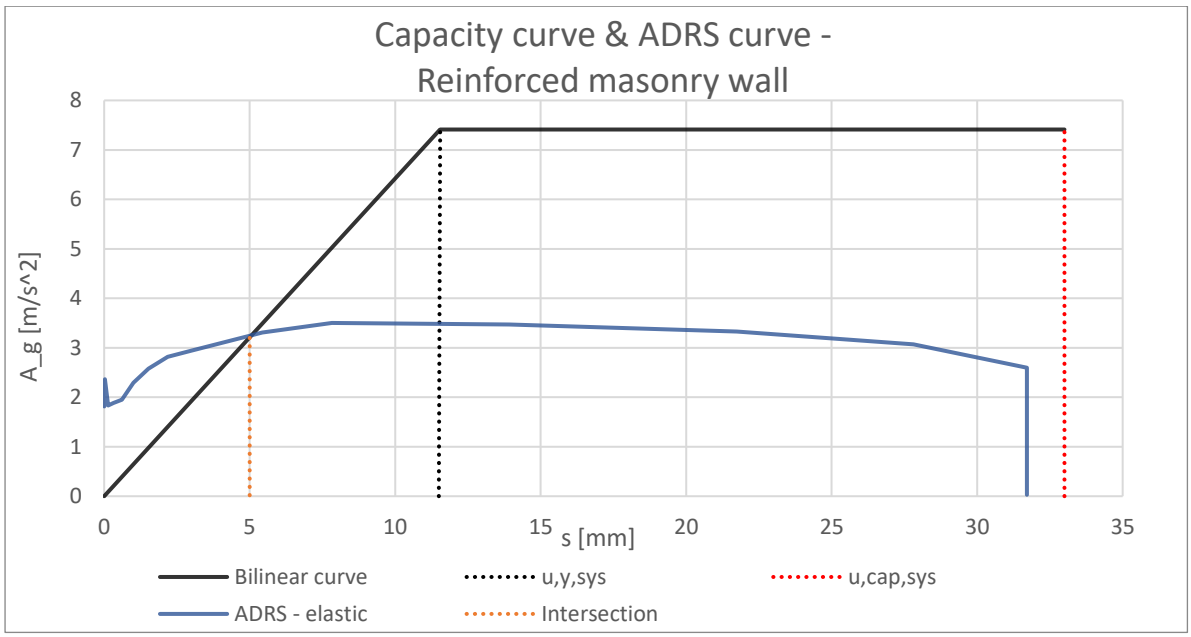

Figure 26: ADRS Curve – Appingedam

In Figure 26 the bilinearization of the capacity curve for the strengthened masonry wall and the ADRS curve of Appingedam is shown for the ULS. This is done by dividing the bilinear curve from Figure 23 with the effective mass of 6000 kg. Since the bilinear curve intersects with the ADRS curve in the elastic region, there is no hysteretic damping or ductile behaviour taking place. The intersection of both curves occurs around 5 mm, this is the actual displacement, whereas the ultimate displacement is 33 mm.

Unreinforced masonry wall

In this section, the pushover calculation is done for the unreinforced masonry wall. The same steps are done and described below.

$m_{eff} = 6000\ kg$
$E_m =$ 1211 Nm , See Table 22

Distance (mm)	Force (kN)	Energy (Nm)
0,6	20	6
18	30,2	437
33	23,2	401
Total		843

Table 23: Overview of the total energy in Nm

$u_{cap;sys} = 33\ mm = 0{,}033\ m$
$F_y = 30\ 200\ N$

$$u_{y;sys} = 2 * \left(u_{cap;sys} - \frac{E_m}{F_y}\right) = 2 * \left(0{,}033 - \frac{843}{30\ 200}\right) = 0{,}0102m = 10{,}2\ mm$$

This gives the following bilinear curve, see Figure 27.

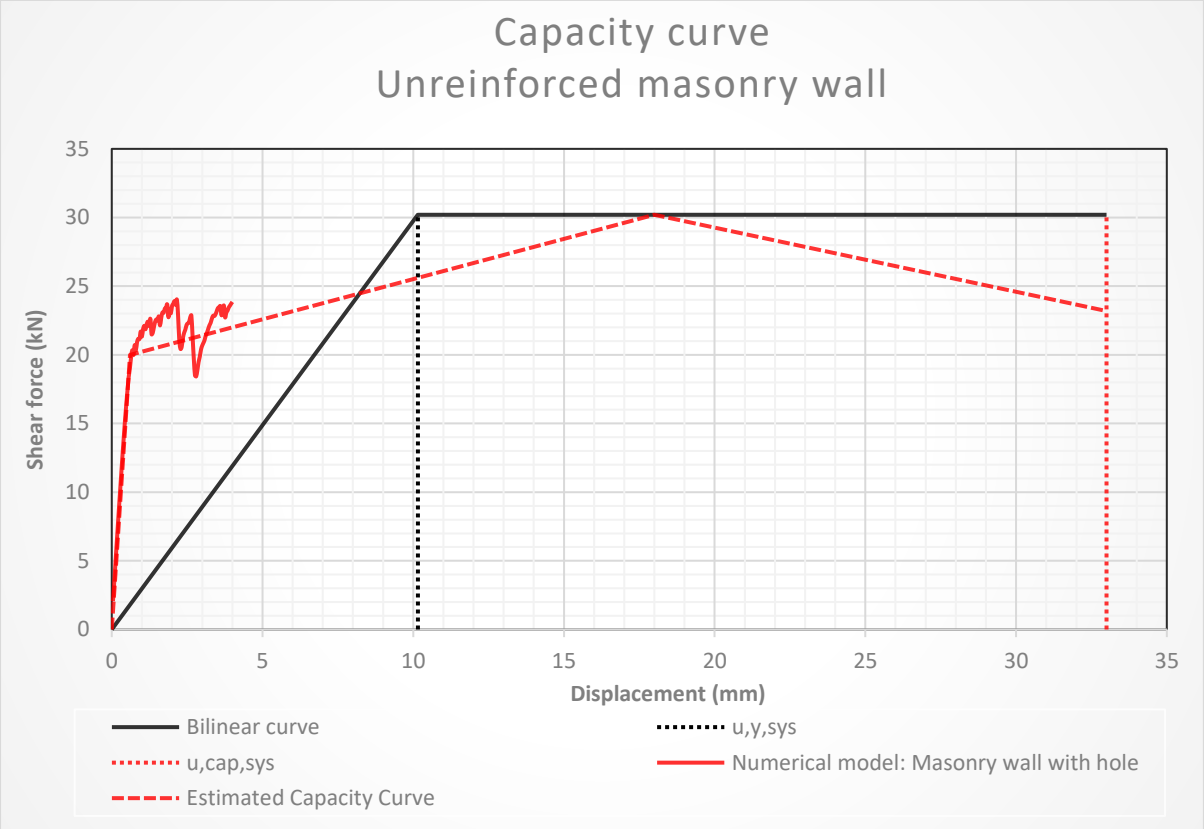

Figure 27: Bilinear capacity curve for the unreinforced masonry wall

$$T_* = 2 * \pi * \sqrt{\frac{m_{eff*} u_{y;sys}}{F_y}} = 0{,}28\ s$$

$$u_{sys} = \frac{u_{duc;sys}}{u_{y;sys}} = \frac{33}{10{,}2} = 3{,}2$$

Now the ductility factor (u_{sys}) is known and the damping factor(ε_{sys}) and the spectral reduction factor(η_ε) can be calculated.

$\varepsilon_{sys} = \varepsilon_0 + \varepsilon_{hys} + \beta_0 \leq 0{,}4$ (40%)
$\varepsilon_0 = inherent\ damping \rightarrow 5\%\ for\ unreinforced\ masonry$

$$\varepsilon_{hys} = hysterical\ damping \rightarrow 0{,}42 * \left(1 - \frac{0{,}9}{\sqrt{u_{sys}}} - 0{,}1 * \sqrt{u_{sys}}\right) \leq 0{,}15$$

$$\varepsilon_{hys} = 0{,}42 * \left(1 - \frac{0{,}9}{\sqrt{u_{sys}}} - 0{,}1 * \sqrt{u_{sys}}\right) = 0{,}135 \leq 0{,}15$$

$\beta_0 = the\ effect\ of\ the\ radiation\ demping\ for\ a\ foundation, this\ can\ be\ neglected\ for\ housing\ of\ two\ buildinglayers.$
$\varepsilon_{sys} = 0{,}05 + 0{,}135 + 0 = 0{,}184 = 18\% \leq 0{,}4$

$$\eta_\varepsilon = \sqrt{\frac{7}{2+\varepsilon_{sys}}} = 0{,}58$$

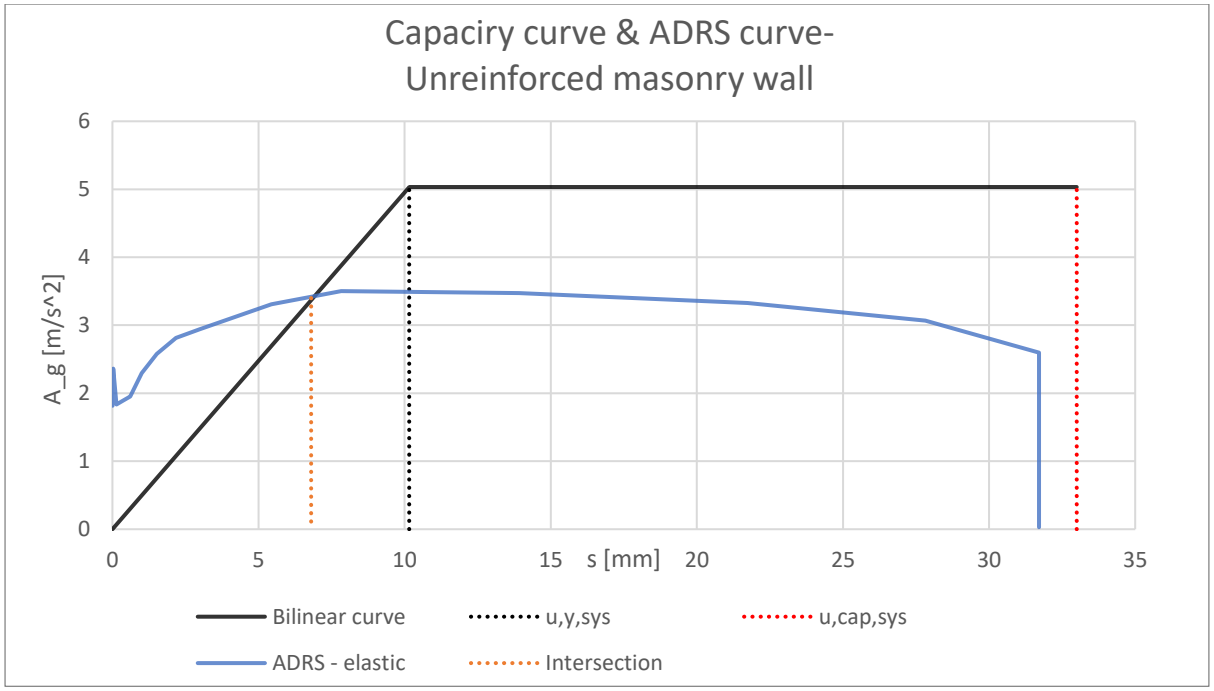

Figure 28: Bilinearisation of a non-linear pushover capacity curve and the ADRS curve

In Figure 28 bilinearization of the capacity curve and the ADRS curve for the ULS of Appingedam is shown in m/s^2. This is done by dividing the bilinear curve from Figure 23 with the effective mass of 6000 kg. Since the Bilinear curve intersects with the ADRS curve in the elastic region, there is no hysteric damping or ductile behaviour of the structure occurring. The intersection of both curves occurs around 6.8 mm, this is the actual displacement, whereas the ultimate displacement is 33 mm.

In Figure 29 the ADRS curves for the ULS and SLS stage and the bilinear capacity curves for the strengthened and unstrengthened walls are shown. Both bilinear curves intersect with the ADRS curves in the elastic region, which means there is no hysteric damping. The intersection of the curves occurs around 1.5, 2, 5 and 6.8 mm, which is the actual displacement, whereas the ultimate displacement is 33 mm. For the ULS the ultimate limit displacement is 33 mm and the actual displacement is 5 and 6.8 mm for the strengthened and unstrengthened wall. For the SLS the actual displacement is 1.5 and 2 mm for the strengthened and unstrengthened wall.

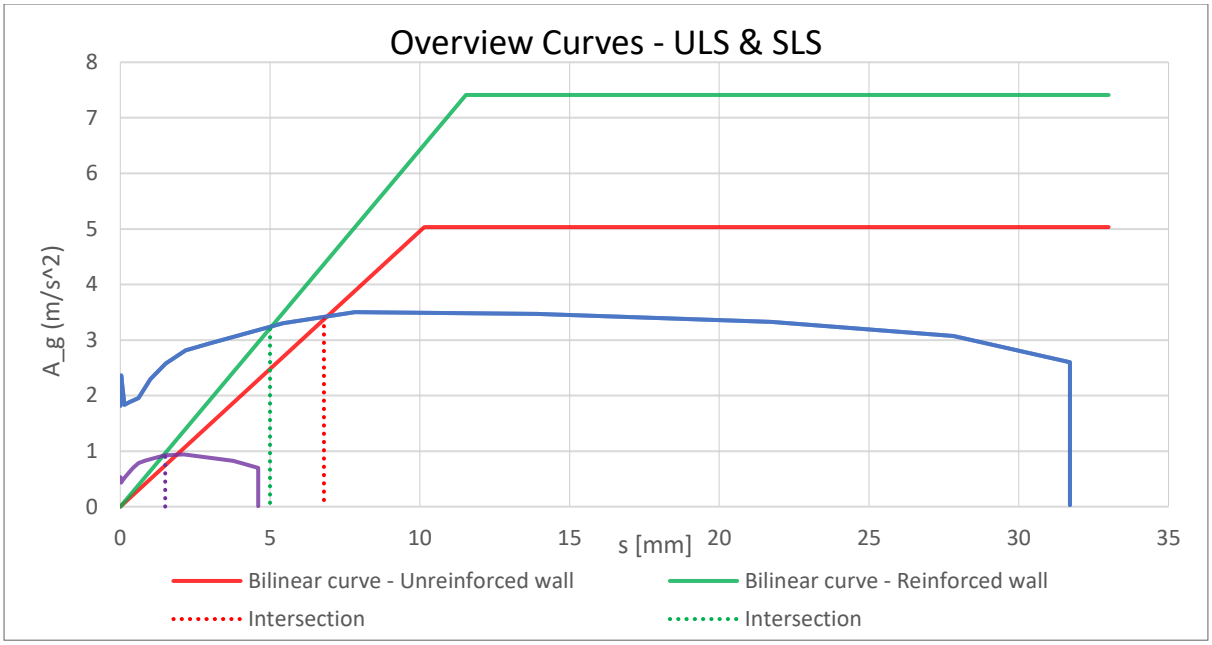

Figure 29: Overview all curves

Different effective mass

To analyse the effect of the effective mass different effective masses are assumed in the calculation. The goal is to include the damping of the ADRS cruve. This is only possible when the bilinear curve is intersecting with the ADRS cruve is the plastic region.

One assumption is that the effective mass is 2400 kg, which is equal to the weight of one masonry wall with the dimensions assumed as in the main rapport. The other assumption is that the effective mass is assumed 150% higher than its original value, which is 15000 kg.

For simplicity reasons only the reinforced masonry walls are calculated and the calculation is not repeated since it is the same calculation.

In Figure 30 and Figure 31 overview of the ADRS curve and the bilinear curves for all different effective masses and the reinforced and unreinforced alternatives are shown for the ULS and SLS. It is noticeable that an effective mass with 2400 kg has a higher peak acceleration than an effective mass of 15000 kg. The bilinear curve of the masonry walls with an effective mass of 2400 kg intersects with the ADRS curve around 1.5 mm, which is still in the elastic region and thus damping is here not included. The bilinear curve of the masonry wall with an effective mass of 15000 kg intersects with the ADRS curve around 29 mm in the plastic region for the ULS. Therefore, the damping of the ADRS curve is included and ductile behaviour of the structure is occurring, see Figure 32. Due to the damping of the ADRS curve, the bilinear curve exceeds the ADRS curve. The

unreinforced masonry wall intersects the bilinear curve as well, however this is at the ultimate limit displacement of 33 mm. For all the curves of the SLS situation the lines intersect in the elastic region and thus no damping is applicable. See the main report for the conclusion.

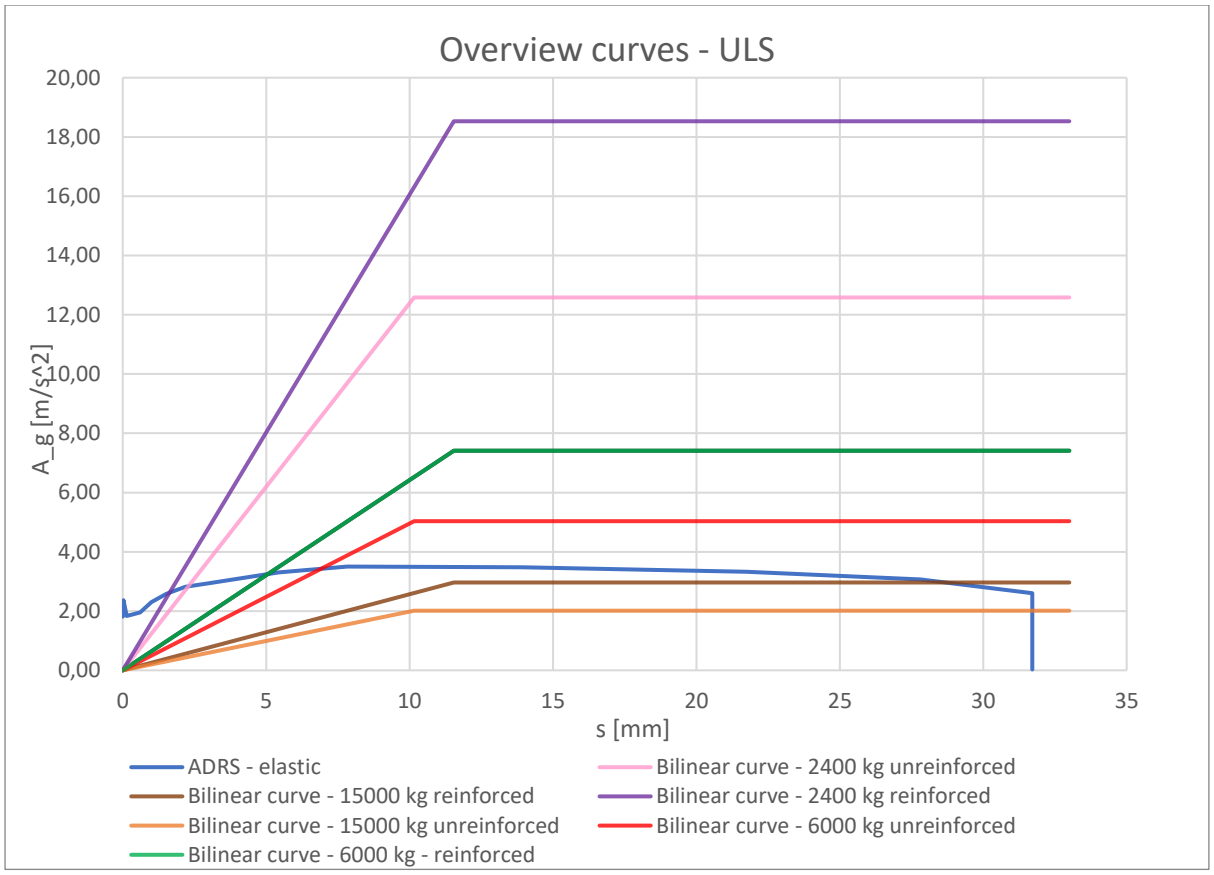

Figure 30: Overview curves for different effective masses in ULS

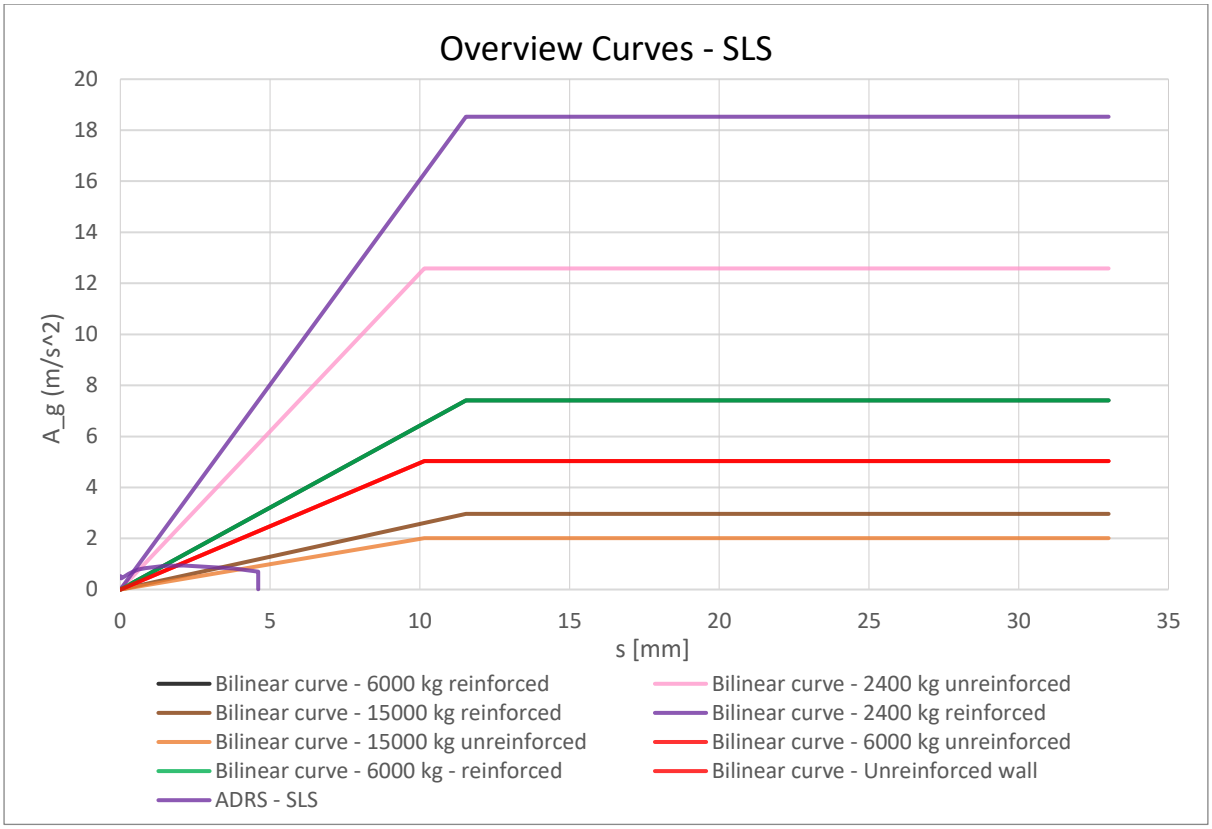

Figure 31: Overview curves for different effective masses in SLS

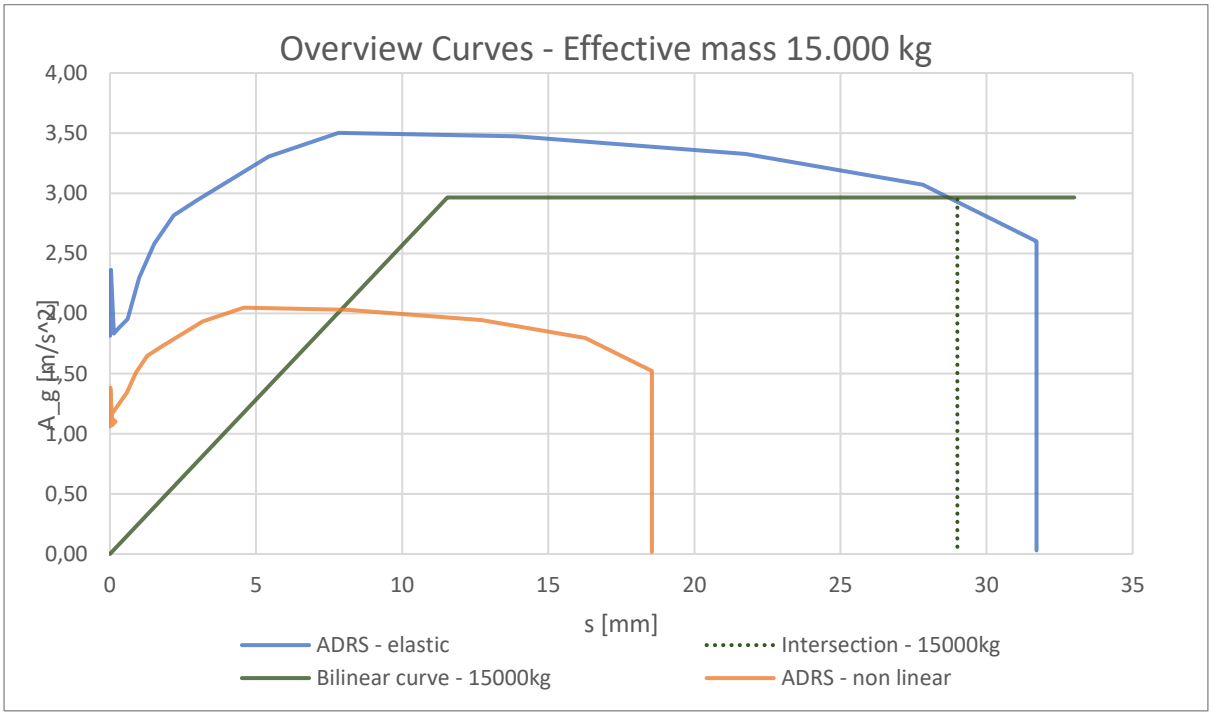

Figure 32: Overview curves for an effective mass of 15.000 kg

E. Drawings

E.1 Drawings of the structural glass window

Window frame: Solid Clay

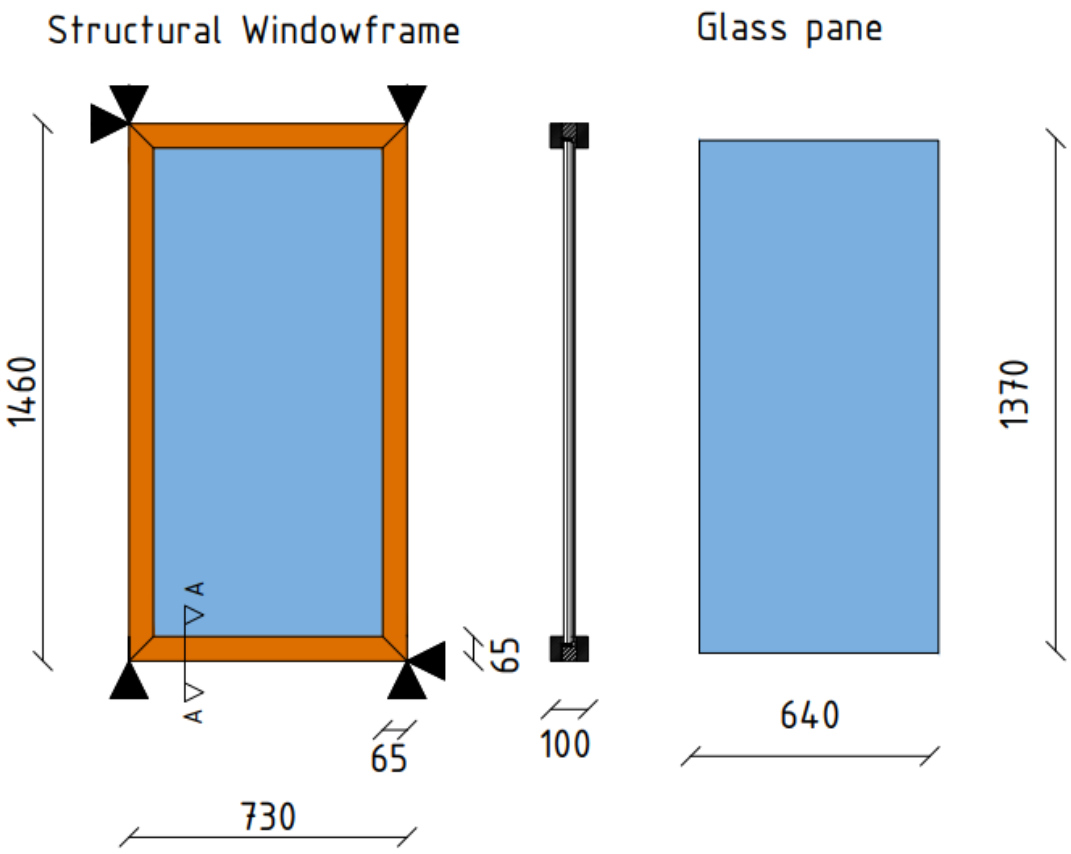

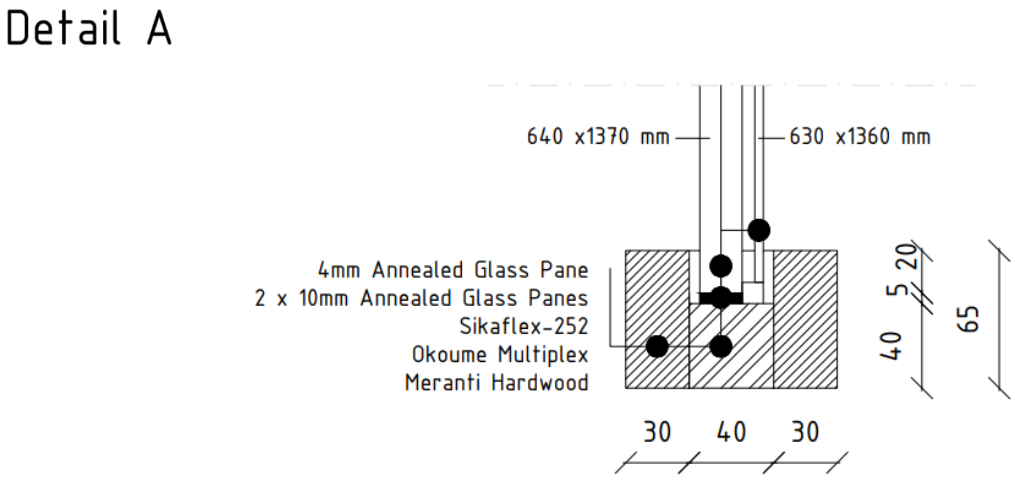

Figure 33: Structural window frame for the solid clay alternative, Glass pane and Detail A

Window frame: Calcium Silicate

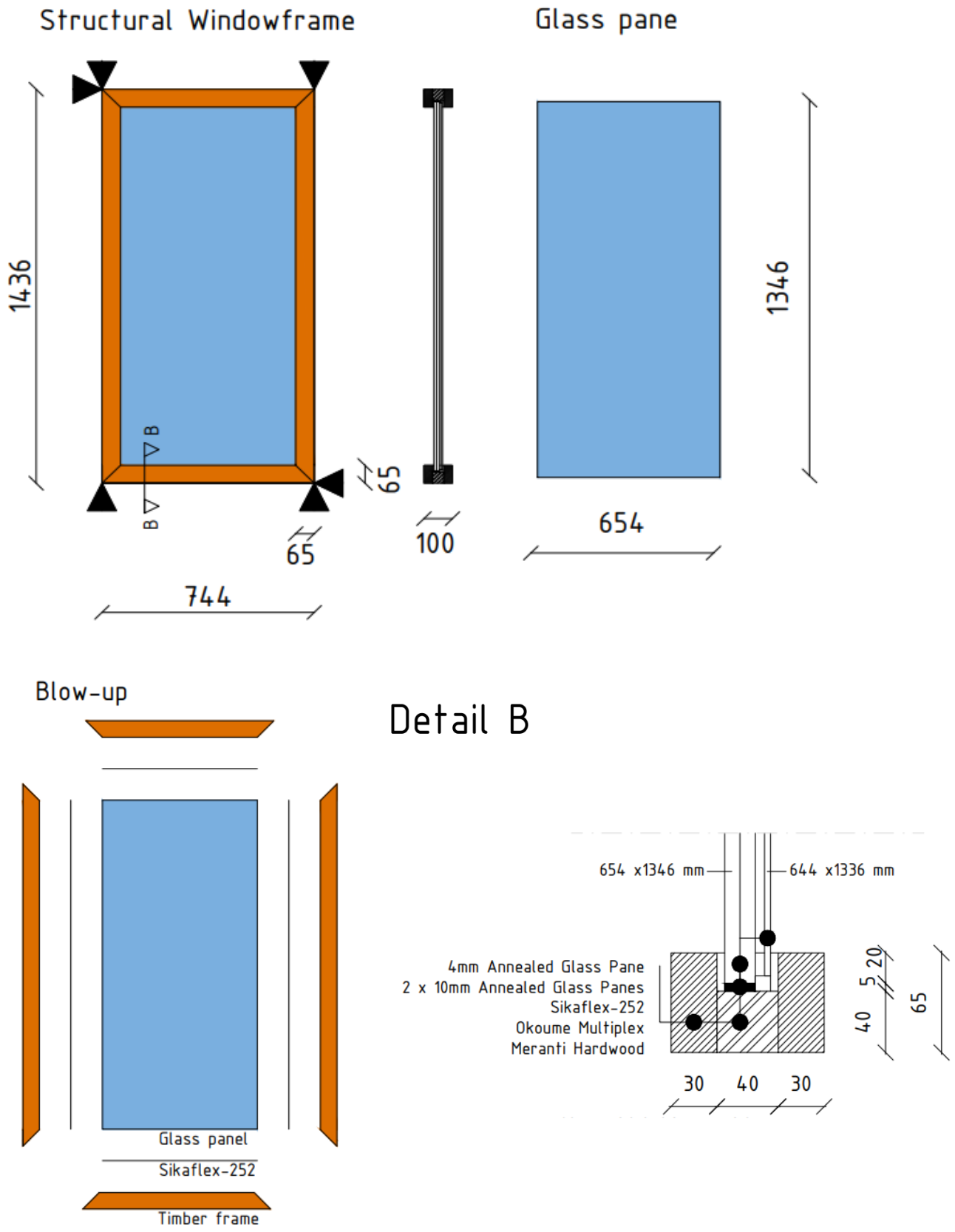

Figure 34: Structural window frame for the calcium silicate alternative, Glass pane and Detail B

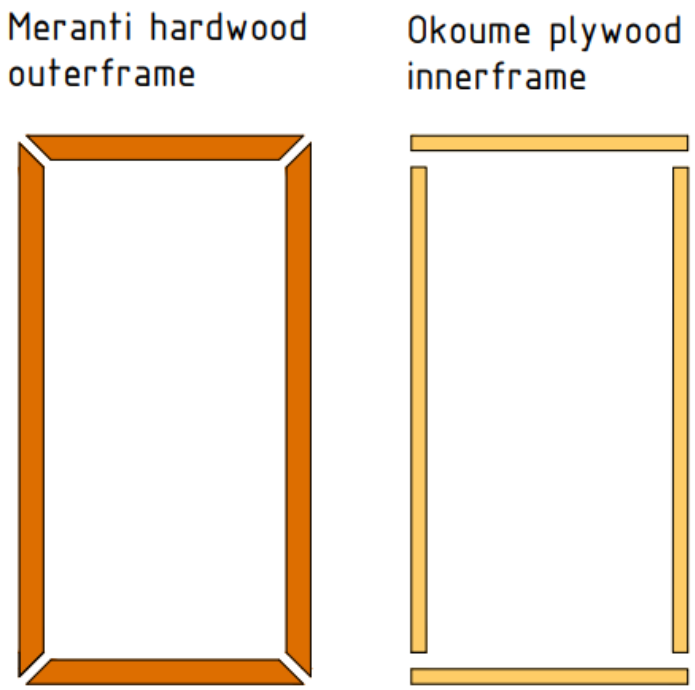

Figure 35: Blow-up and built up of the timber frame

F. Design study

F.1 Increase stiffness of the timber frame

The same calculation is done as described in Attachment C.1. For the calculation, it is assumed that the plywood is twice as stronger as in the original design. This way the influence of a stronger and stiffer timber frame is investigated.

Overview stress for the twice as stiff timber frame

Relative Interface Displacement	Maximum Stress Glass
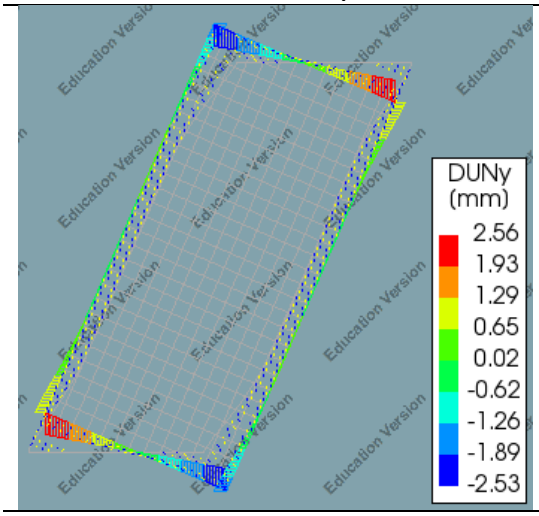	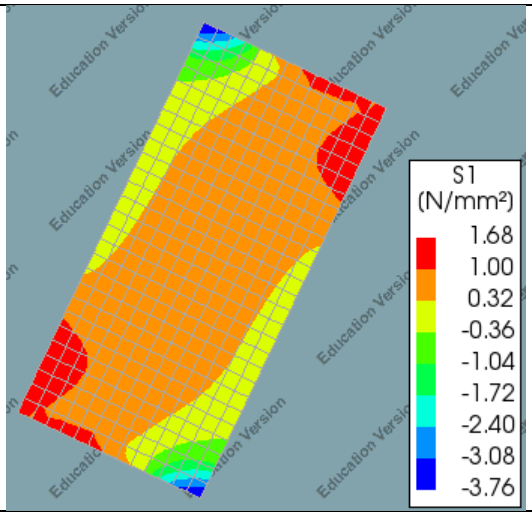
Total Displacement: 14 mm Relative Interface displacement: +2,5 mm	
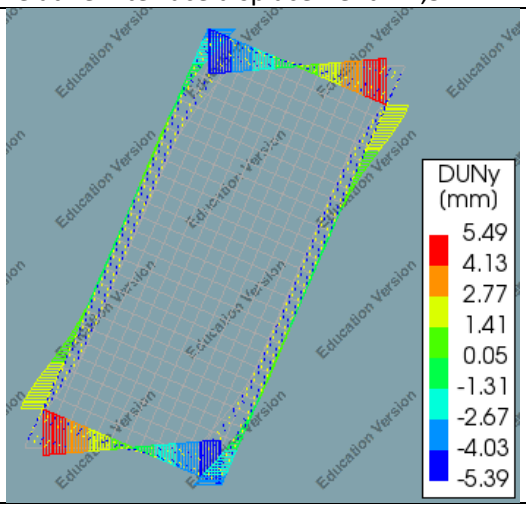	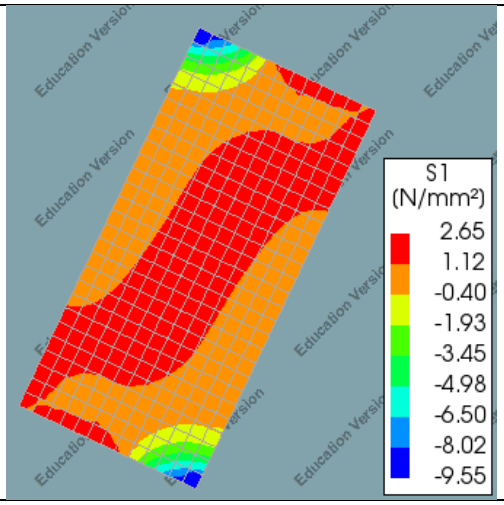
Total Displacement: 30 mm Relative Interface Displacement: -5,3 mm	
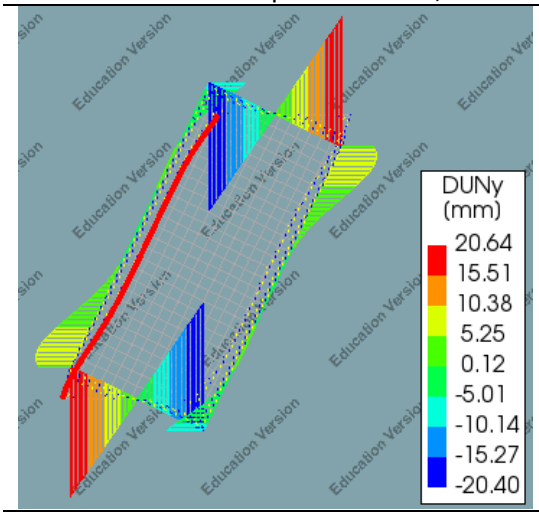	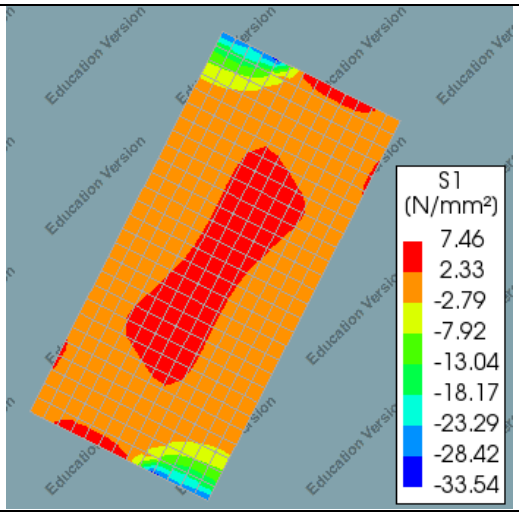
Total Displacement: 100 mm	Maximum stress:

Table 24: Relative interface displacement versus the maximum stress inside the glass panel

F.2 Thinner adhesive

Timber stiffness properties		
u_2 (mm)	σ_2 (N/mm^2)	k_2 (N/mm^3)
-	-15	-
-	-15	-
-6	-15	2.5
-1.6	-21.8	13,6
-0.5	-18	36
-0.024	-0.9	37.5
0	0	0
-	-	-
-	-	-
-	-	-

Table 25: Serial spring stiffness properties for a structural window frame with an adhesive layer of 0 mm

Overview stress for the model with 3 mm adhesive

Relative Interface Displacement	Maximum Stress Glass
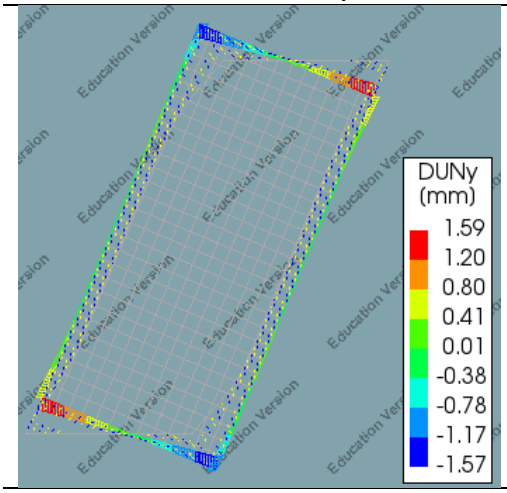	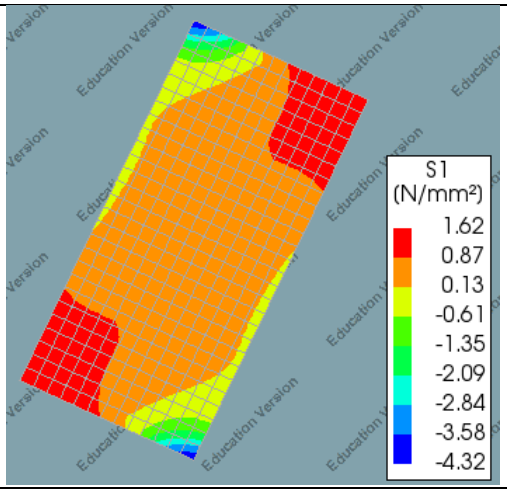
Total Displacement: 9 mm Relative Interface displacement: +1,5 mm	Phase 1b: Tearing of the adhesive
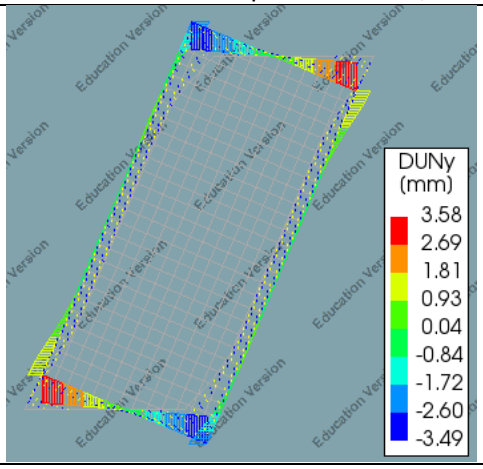	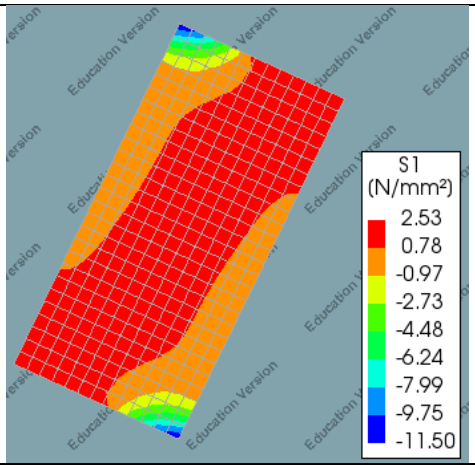
Total Displacement: 20 mm Relative Interface Displacement: -3.5mm	Phase 2: Intersection Glass/timber frame
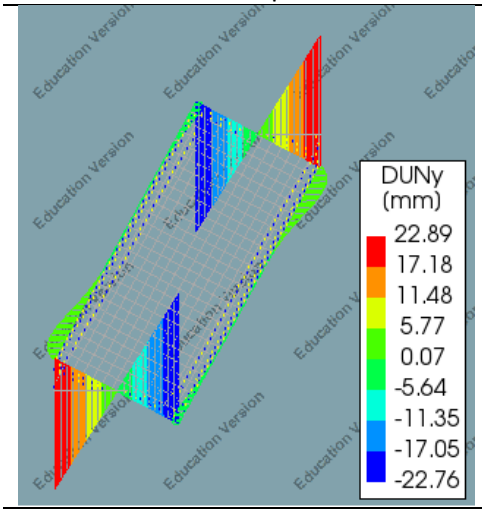	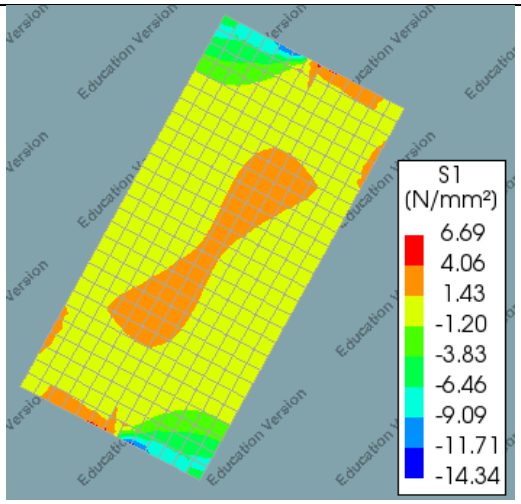
Total Displacement: 100 mm	Maximum stress: + 7MPa

Table 26: Relative interface displacement versus the maximum stress inside the glass panel

Overview stress for the model with no adhesive

Relative Interface Displacement	Maximum Stress Glass
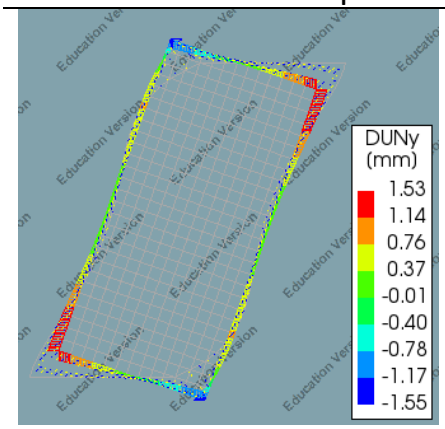	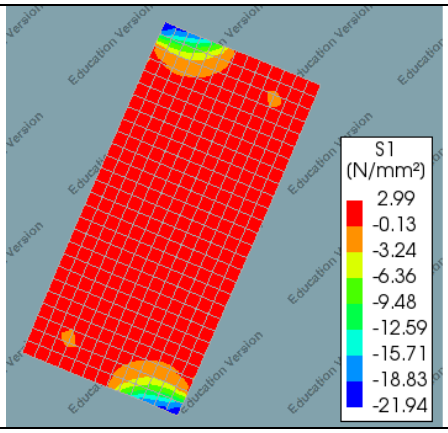
Total Displacement: 9 mm	
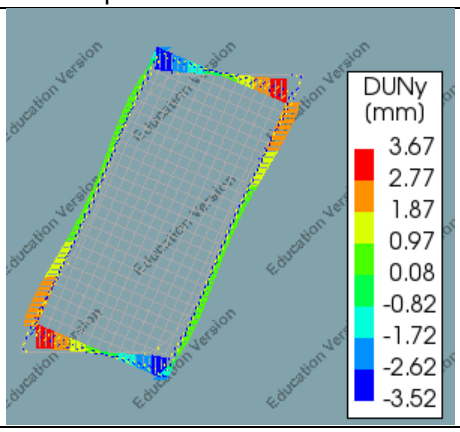	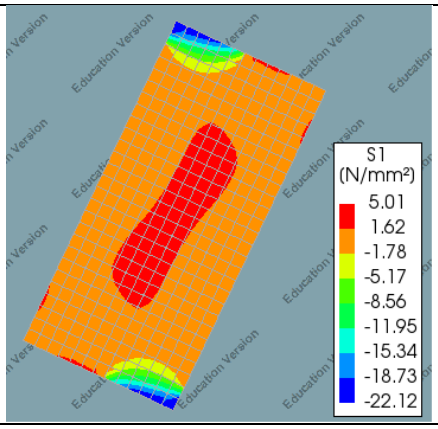
Total Displacement: 20 mm	Phase 2: Intersection Glass/timber frame
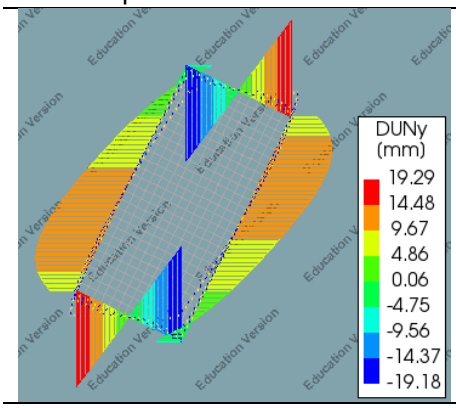	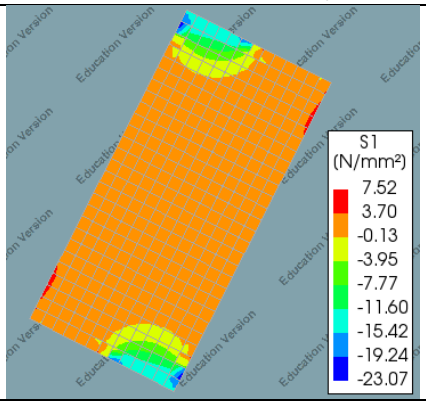
Total Displacement: 93 mm	Maximum stress: + 7 MPa

Table 27: Relative interface displacement versus the maximum stress inside the glass panel

Overview of the numerical masonry model for different adhesive thicknesses

Numerical masonry model : Structural façade – 5 mm adhesive	**Numerical masonry model : Structural façade – 3 mm adhesive**	**Numerical masonry model : Structural façade – No adhesive**
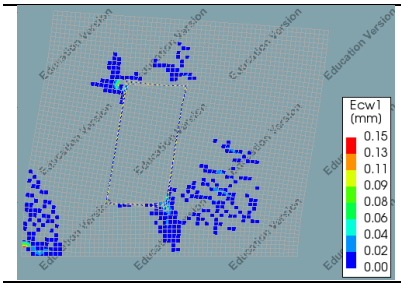	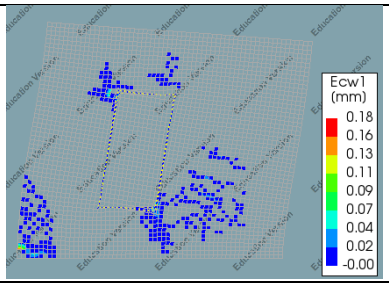	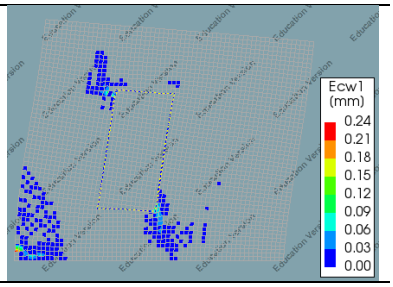
End of the Linear elastic stage Loadstep 18: 0.68 mm displacement		
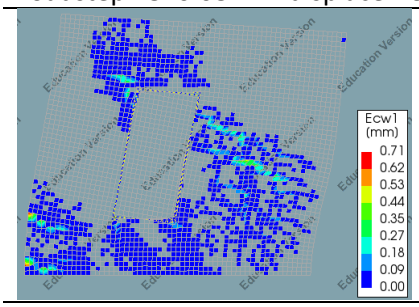	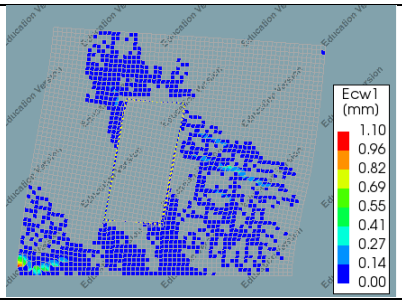	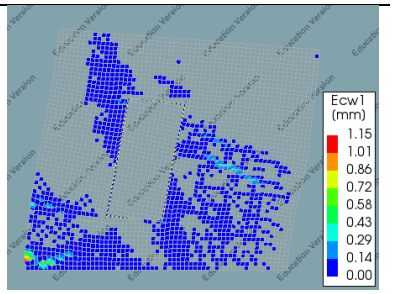
End of the experiment Loadstep 40: 1.56 mm displacement		
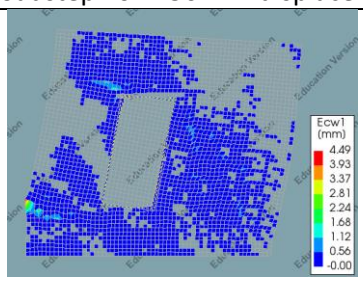	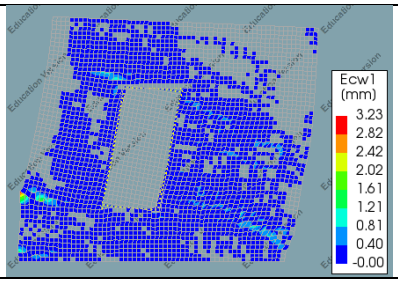	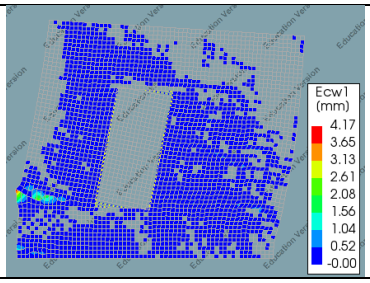
End of the numerical model Loadstep 100: 4 mm displacement		

Table 28: Crack width for different numerical masonry models

F.3 Demountable timber frame

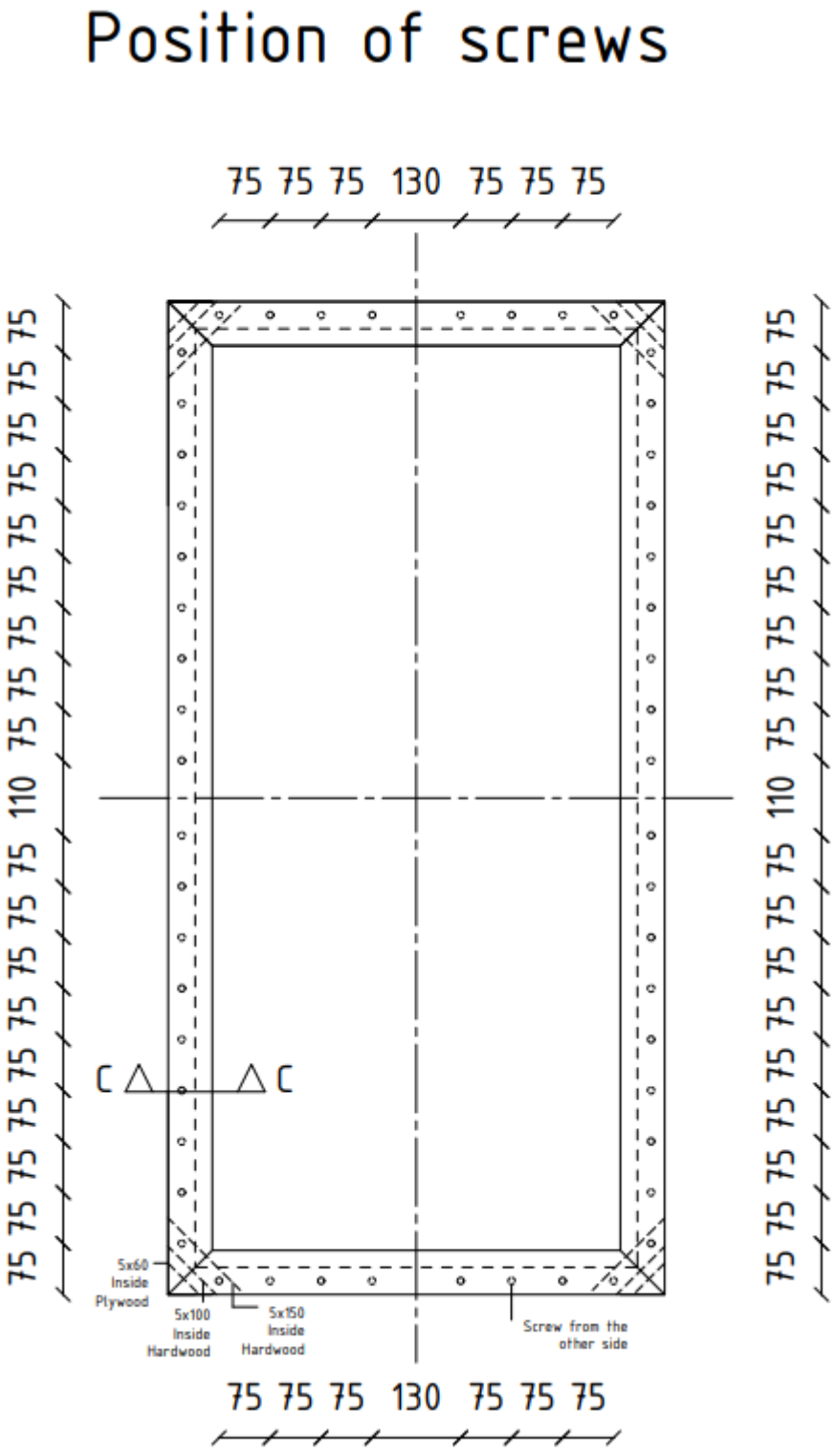

Figure 36: Positioning of screws

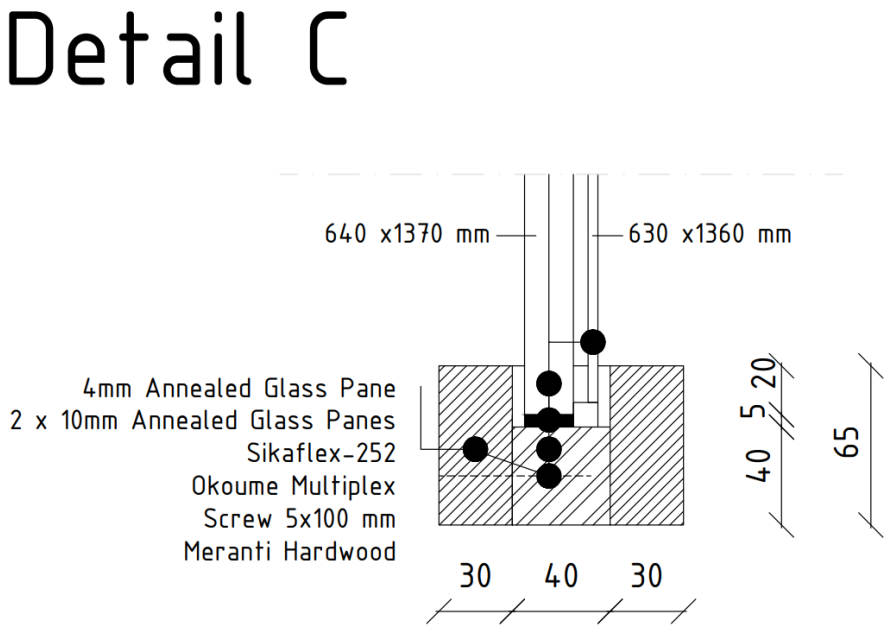

Okoume plywood innerframe

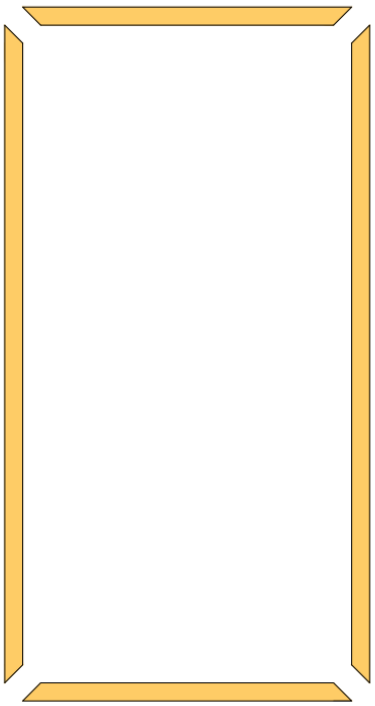

Figure 37: Top – Detail C, Bottom – adjusted design for the inner frame